BERKELEY RESEARCH ASSOCIATES, INC.

AFOSR-TR- 88-0977

BRA-89-W010R

July 1988

MODELING OF ATOMIC PROCESSES FOR X-RAY LASER PLASMAS

FINAL REPORT
Contract No. F49620-86-C-0076

Period of Performance
June 1986 - February 1988

for

Air Force Office of Scientific Research
Bolling Air Force Base
Washington, D.C. 20332-6448

by

Berkeley Research Associates, Inc.
P.O. Box 852
Springfield, VA 22150

UNCLASSIFIED
SECURITY CLASSIFICATION OF THIS PAGE

AD-A200219

REPORT DOCUMENTATION PAGE

Form Approved
OMB No. 0704-0188

1a. REPORT SECURITY CLASSIFICATION UNCLASSIFIED	1b. RESTRICTIVE MARKINGS
2a. SECURITY CLASSIFICATION AUTHORITY	3. DISTRIBUTION/AVAILABILITY OF REPORT Approved for public release; distribution is unlimited.
2b. DECLASSIFICATION/DOWNGRADING SCHEDULE	
4. PERFORMING ORGANIZATION REPORT NUMBER(S)	5. MONITORING ORGANIZATION REPORT NUMBER(S) AFOSR-TR- 88-0977
6a. NAME OF PERFORMING ORGANIZATION Berkeley Research Associates 6b. OFFICE SYMBOL (If applicable)	7a. NAME OF MONITORING ORGANIZATION AFOSR/NP
6c. ADDRESS (City, State, and ZIP Code) P.O. Box 241 Berkeley, CA 94701	7b. ADDRESS (City, State, and ZIP Code) Building 410, Bolling AFB DC 20332-6448
8a. NAME OF FUNDING/SPONSORING ORGANIZATION AFOSR 8b. OFFICE SYMBOL (If applicable) NP	9. PROCUREMENT INSTRUMENT IDENTIFICATION NUMBER F49620-86-C-0076
8c. ADDRESS (City, State, and ZIP Code) Building 410, Bolling AFB DC 20332-6448	10. SOURCE OF FUNDING NUMBERS PROGRAM ELEMENT NO. 61102F; PROJECT NO. 2301; TASK NO. A8; WORK UNIT ACCESSION NO.

11. TITLE (Include Security Classification)

(U) MODELING OF ATOMIC PROCESSES IN X-RAY LASER PLASMAS

12. PERSONAL AUTHOR(S)

Dr. Uday Gupta

13a. TYPE OF REPORT	13b. TIME COVERED	14. DATE OF REPORT (Year, Month, Day)	15. PAGE COUNT
FINAL	FROM 6/15/86 TO 2/14/88	July 1988	74

16. SUPPLEMENTARY NOTATION

17. COSATI CODES			18. SUBJECT TERMS (Continue on reverse if necessary and identify by block number)
FIELD	GROUP	SUB-GROUP	Photoionization, Photoexcitation, Plasmas, Multielectron
20	09		

19. ABSTRACT (Continue on reverse if necessary and identify by block number)

This work dealt with the theoretical modeling and computation of photoionization, photo-excitation, radiative decay and radiative recombination processes for multielectron atoms and ions in plasmas. Such atomic processes lead to and influence lasing in x-ray lasers operating both in the soft and hard x-ray regions. This research utilized a two-component, finite temperature, self consistent density functional method and demonstrated that this method is applicable for arbitrary plasma density and temperature and is capable of accurately treating multielectron ions of arbitrary Z. Electron collisional ionization and excitation processes were investigated. These processes are an important mechanism through which population inversion of ionic energy levels lead to lasing in the soft x-ray region. Previously theoretical calculations utilizing a semi-classical impact approximation have been performed. In many cases such a method is inadequate. Computations were carried out by electron impact ionization and excitation cross-sections and rate coefficients utilizing the distorted wave with exchange method.

20. DISTRIBUTION/AVAILABILITY OF ABSTRACT	21. ABSTRACT SECURITY CLASSIFICATION
X ☐ UNCLASSIFIED/UNLIMITED X ☐ SAME AS RPT. ☐ DTIC USERS	UNCLASSIFIED
22a. NAME OF RESPONSIBLE INDIVIDUAL Dr Robert J Barker	22b. TELEPHONE (Include Area Code) (202) 767-5011
22c. OFFICE SYMBOL AFOSR/NP	

DD Form 1473, JUN 86 — Previous editions are obsolete. — SECURITY CLASSIFICATION OF THIS PAGE

UNCLASSIFIED

BRA-89-W010R

July 1988

MODELING OF ATOMIC PROCESSES

FOR

X-RAY LASER PLASMAS

FINAL REPORT
Contract No. F49620-86-C-0076

Period of Performance
June 1986 - February 1988

for

Air Force Office of Scientific Research
Bolling Air Force Base
Washington, D.C. 20332-6448

by

Berkeley Research Associates, Inc.
P.O. Box 852
Springfield, VA 22150

BERKELEY RESEARCH ASSOCIATES, INC.
P.O. Box 852 Springfield, Virginia 22150 703/750-3434

BRA-89-W010R
July 1988

MODELING OF ATOMIC PROCESSES

FOR

X-RAY LASER PLASMAS

FINAL REPORT
Contract No. F49620-86-C-0076

Period of Performance
June 1986 - February 1988

for

Air Force Office of Scientific Research
Bolling Air Force Base
Washington, D.C. 20332-6448

by

Berkeley Research Associates, Inc.
P.O. Box 852
Springfield, VA 22150

TABLE OF CONTENTS

EXECUTIVE SUMMARY

This final report presents research carried out by Berkeley Research Associates, Inc. under Contract F49620-86-C-0076 with the Air Force Office of Scientific Research (AFOSR). The report covers the performance period June 1986 through February 1988. During this period we carried out research on the modeling of atomic processes for x-ray laser plasmas. The report is divided into two parts. Part I covers research performed from June 1986 through July 1987 and Part II covers research performed from August 1987 through Februar 1988.

In Part I, we deal with the theoretical modeling and computation of photoionization, photoexcitation, radiative decay and radiative recombination processes for multielectron atoms and ions in plasmas. Such atomic processes lead to and influence lasing in x-ray lasers operating both in the soft and hard x-ray regions. Most previous calculations for multielectron ions have used a single electron or independent particle model. Although comparison of experimental data with such models shows agreement for simple systems such as a neutral few-electron atom, substantial discrepancies are found for many electron atoms and ions with a large number of bound electrons. In our research we utilized a two-component, finite temperature, self consistent density functional method and demonstrate that this method is applicable for arbitrary plasma density and temperature and is capable of accurately treating multielectron ions of arbitrary Z.

In Part II, we investigate electron collisional ionization and excitation processes. These processes are an important mechanism through which population inversion of ionic energy levels lead to lasing in the soft x-ray region. Previously theoretical calculations utilizing a semi-classical impact approximation have been performed. In many cases such a method is inadequate. In our research, we carried out computation of electron impact ionization and excitation cross-sections and rate coefficients utilizing the distorted wave with exchange method. We found that this approach provides a speedy and reasonably accurate tool for these calculations.

PART I

MODELING OF ATOMIC PROCESSES

FOR

X-RAY LASER PLASMAS

TABLE OF CONTENTS

I. INTRODUCTION

Development of X-ray lasers operating both in the soft and hard X-ray region is currently an area of intensive research. A variety of atomic processes lead to and influence lasing action in such systems. Photoionization, photoexcitation, radiative decay and radiative recombination are some of these processes. This report deals with the theoretical modeling and computation of the above mentioned processes for multielectron atoms and ions in plasmas.

Accurate calculation of photoionization and photoexcitation cross-sections of atoms and ions are useful in a variety of investigations in plasma physics and atomic physics. It is particularly useful in the context of photopumping schemes for X-ray lasers. As another example, computation of opacities of plasmas for diagnostic and target response effects require these data as input. In order to model the radiation spectra from hot plasmas (via the detailed configuration rate equation for example), these data are required along with the other bound-bound, bound-free and free-free processes. Radiative recombination and radiative decay rates are very useful in X-ray laser research - particularly in the context of recombination schemes. In view of these different applications, there is a need for realistic modeling of these processes to generate accurate data for a variety of atoms and ions.

In a large number of existing calculations, the above processes have been calculated using simple approximate formulae, valid for hydrogenic ions only. Depending on plasma conditions, however, multielectron ions (Ne-like ion, for example, with ten electrons bound to it) may have a much higher abundance than hydrogenic ions. Most calculations for multielectron ions existing in the literature have been done using the single electron or independent particle model (IPA). In this model, the energy levels and wavefunctions of the atom or ion are first calculated using the Hartree-Fock (HF) method. For photoionization calculation, the interaction of the incident electromagnetic radiation with the atom (or ion) is treated via the first order perturbation theory[1].

Comparison of experimental data with the IPA calculations shows that for some simple systems such as a neutral few-electron atom (Lithium, for example), there is qualitative, sometimes quantitative agreement. However, for many electron atoms (Xenon, for example) and ions with a large number of bound electrons, substantial discrepencies are found between experimental and IPA-data[1].

In our work, we used the time dependent linear response approximation within the framework of relativistic local density functional method (DFM)[2,3,4] to treat the problem of photoionization. This method incorporates several advantages over the HF-method. The HF-method is non-local and computationally very elaborate, whereas in the

density functional method, one deals with a set of local equations only. This leads to computational simplicity. On the other hand, from extensive applications of the density functional method (DFM) it is well known that fairly accurate atomic energy levels, wavefunctions etc. are obtained[14]. The computational simplicity is even more apparent in the case of relativistic DFM versus relativistic HF-methods, (proper treatment of high Z atoms require the application of the relativistic DFM). In the DFM, correlation effects of the bound electrons in the atom are accounted for in a simple way via the correlation potential[5]. The HF-method, on the other hand, does not take into account electron correlation, although it accounts for non-local exchange effects appropriately.

For photoionization and photoexcitation process (and therefore for radiative recombination, since this is effectively the inverse of photoionization), the polarization effect of the atom brought about by the incident radiation field is important. The independent particle method does not take this into account. In the linear response method within the DFM we have used in this work, this effect is treated adequately - as will be seen from comparison with experimental data. In most experimental situations, the incident radiation (from synchrotron sources or lasers) have field strengths small compared to the atomic field strengths. For those experimental conditions, the present model based on linear response is adequate and useful.

The above discussion deals with the calculation of atomic structure and processes for an isolated atom or ion - that is, without the effect of the plasma environment. This is valid for very low density plasmas. As the plasma density increases, several additional effects such as the screening shifts of energy levels (or lowering of ionization potential) and modification of wave-functions and potentials for the ion embedded in high density plasmas have to be considered. The effect of plasma density on the atomic (or ionic) structure and atomic processes needs to be properly investigated. In the present work, we investigated these effects via the two-component finite temperature self-consistent DFM[6] and compared the results with corresponding isolated ion calculations.

The study of plasma density (and temperature) effect is also important to determine the optimum operating conditions for gain enhancement in X-ray lasers. At very low plasma density, collisional excitation and deexcitation rates are small; radiative decay is then a dominant process. However, as the plasma density increases, the collisional rates increase rapidly and collisional radiative equilibrium can exist. These in turn, have their effects on the relative abundance of ionic population as well as on the population inversion of ionic levels and thus affect lasing. The investigation of plasma density and temperature effects on atomic processes is therefore, of importance in overall X-ray laser modeling.

The self-consistent two component DFM method we have used provides a useful tool for realistic modeling of the various effects arising in high density hot plasmas. The electron degeneracy effect is correctly treated via the Fermi distribution function and the exchange-correlation effect of bound and free electrons are taken into account via the exchange-correlation potential. The two-component scheme generates the ion distribution self-consistently along with the electron distribution. The approximations of "average atom" models such as Thomas Fermi[7] are avoided - leading to much more accurate ionic potential, bound and free electron distributions and the specific ionic configuration. The screening effect is treated in our model in a fully non-linear fashion - unlike Debye-screening, which is known to be inadequate for screening by bound electrons. The two-component DFM is applicable for arbitrary plasma density and temperature and is capable of treating multielectron ions of arbitrary Z accurately.

II. THE METHOD OF CALCULATION

a. Isolated Atoms or Multielectron Ions

When the plasma density is very low, the atoms or ions forming the plasma can be considered as practically non-interacting or isolated from each other. The bulk of the existing atomic data used in X-ray laser modeling by different research groups have been calculated for isolated ions. In our modeling, we have used the local density functional method (DFM) for that purpose. In actual calculations, in order to treat many electron atoms with high z appropriately, relativistic DFM was used. For purposes of simplicity, we discuss the non-relativistic DFM in this section. The relativistic DFM is discussed in Reference 4.

The first part of the calculation is to generate the energy-level spectrum and the wave-functions of the particular atom or ion of specific configuraiton. In the non-relativistic DFM, the following set of equations were solved iteratively to self-consistency:

$$\left(-\frac{1}{2}\nabla^2 + V_a(\vec{r})\right)\Psi_i(\vec{r}) = \varepsilon_i \Psi_i(\vec{r}) \tag{1}$$

$$V_a(\vec{r}) = -\frac{Z}{r} + \int \frac{n(\vec{r}')d\vec{r}'}{|\vec{r}-\vec{r}'|} + V_{xc}(\vec{r}) \tag{2}$$

and

$$n(\vec{r}) = \sum_i f_i |\Psi_i(\vec{r})|^2 \qquad (3)$$

In above n(r) is the electronic charge density of the atom or multielectron ion, f_i's are the integral occupation factors corresponding to the number of electrons in each state $\Psi_i(r)$ with corresponding energy eigenvalue ε_i. The atomic potential $V_a(r)$ contains, in addition to the nuclear and the electrostatic Hartree term, a contribution arising from the exchange-corelation effects (V_{xc}) due to interaction among bound electrons. Let us note that the integer occupation factors f_i's for the giren configuration distinguishes this model from the "average atom model" in which the occupation factors are taken to be those given by the statistical fermi distribution function.

The exchange-correlation potential V_{xc} has to be calculated separately from many-body theory and used as an input here. In our calculation, Gunnarsson-Lundquist (G-L) form for V_{xc} was used. It is known that reliable atomic data is obtained from G-L exchange-correlation. Eqs. (1)-(3) were solved numerically to self-consistency to obtain the wavefunctions Ψ_i's, the binding energies ε_i's of each orbital, the atomic charge density $\rho(r)$ and the self-consistent potential $V_a(r)$.

To calculate the photoabsorption by the atom (or ion), now consider the effect of an incident time-varying radiation field $E(t)=E_o e^{i\omega t}$ on the atom. It induces a time dependent atomic density deviation, $\delta n(\vec{r},t)$, causing a time-

dependent polarization effect. For the linear response method used here, it is convenient to work with the Fourier transform:

$$\delta n(\vec{r},t) = \frac{1}{2\pi} \int_{-\infty}^{\infty} \delta n(\vec{r},\omega) e^{-i\omega t} \, d\omega \qquad (4)$$

the net induced density due to the external plus the induced potential is:

$$\delta n_{ind}(\vec{r},\omega) = \int \chi(\vec{r},\vec{r}',\omega) \left[V_{ext}(\vec{r},\omega) + V_{ind}(r,\vec{\omega}) \right] d\vec{r}', \qquad (5)$$

where the induced potential is given by

$$V_{ind}(\vec{r},\omega) = \int \frac{\delta n(\vec{r}',\omega)}{|\vec{r}-\vec{r}'|} \, d\vec{r}' + \frac{\partial V_{xc}(n(\vec{r}))}{\partial n(\vec{r})} \delta n(\vec{r},\omega) \qquad (6)$$

The response function is given by

$$\chi(\vec{r},\vec{r}',\omega) = \sum_i f_i \Psi_i^*(\vec{r}) \Psi_i(\vec{r}') \, G(\vec{r},\vec{r}', \varepsilon_i + \hbar\omega)$$

$$+ \sum_i f_i \Psi_i(\vec{r}) \Psi_i^*(\vec{r}') G^*(\vec{r},\vec{r}', \varepsilon_i - \hbar\omega) \qquad (7)$$

and thus involves the wave functions and energy levels of the atom. The Green's functions are solutions of the inhomogeneous Schrodinger equation and are constructed numerically.

The frequency dependent polarizability $\alpha(\omega)$ is the ratio of the induced dipole moment to the external field:

$$\alpha(\omega) = -\frac{e}{E_o}\int z\ \delta n(\vec{r},\omega)d\vec{r} \tag{8}$$

Note that $\alpha(\omega)$, like $\delta n(r,\omega)$ is complex. The induced density deviation (and the corresponding induced potential) can have a phase difference with respect to that of the applied external field. Once $\alpha(\omega)$ is determined, the photoabsorption cross-section $\sigma(\omega)$ of the atom or the ion is calculated from:

$$\sigma(\omega) = \frac{4\pi\omega}{c}\ \mathrm{Im}\ \alpha(\omega) \tag{9}$$

b. Partial Cross-Section

Eq. (9) gives the total photoabsorption cross-section which is the sum of partial (individual) photoionization cross-sections. To see the connection with the IPA-model, consider the partial cross-section due to photoionization from a specific bound state $\psi_i(r)$.

The initial atomic state is represented as

$$\Psi_i(\vec{r}) = \frac{U_{nl}(r)}{r} Y_l(\hat{r}) \tag{10}$$

and the final continuum state with wave vector $\vec{K}$ and energy ε as

$$\Psi_f(\vec{r}) = 4\pi \sum_{l'} A_{l'} i^{l'} \frac{P_{\varepsilon l'}(r)}{r} Y_{l'}^{*}(\hat{K}) Y_{l'}(\hat{r}) \qquad (11)$$

The complex coefficients A_l's are found by requiring $\Psi_f(r)$ to behave aasumptotically as an incident plane wave plus a spherical wave. Then the partial cross-section σ_{nl} is shown to be

$$\sigma_{nl}(\omega) = 2(2l+1)\alpha\hbar\omega \sqrt{\varepsilon}\, a_B^2$$
$$\times \sum_{l'} |A_{l'}|^2 |\langle l\ 100\ |\ l'o\rangle|^2 \left| \int P_{\varepsilon l'}(r) V^{SCF}(r,\omega) u_{nl}(r) dr \right|^2 \qquad (12)$$

where $\langle l\ 100\ |l'o\rangle$ is a clebsch-Gordon coefficient.

In (12), $V^{SCF}(r,\omega)$ is a frequency dependent complex self-consistent potential generated in solving iteratively Eq. (5) - (7). Note that, if $V^{SCF}(r,\omega)$ is replaced by the usual dipole moment operator, one obtains the conventional or independent particle approximation (IPA) result. Also, the real and imaginary parts of the self-consistent field contributes to the partial cross-section without interference.

c. Radiative Decay

The Einstein transition probability rate is defined as the total probability per unit time of an atom in a specific state i making a transition to a final state j. The wave functions and energy levels for the atom (or ion) were first generated using the atomic structure code. The radiative decay rate were then calculated by evaluating the relevant dipole matrix element numerically for the particular transition. The actual equations are given in Ref. 12. We used (j-j) coupling in our calculations.

d. Radiative Recombination

This is effectively the inverse of photoionization process. Thus, once the photoionization cross-sections have been computed as discussed earlier, the readiative capture cross-sections (and rates) can then be calculated from the process of detailed balance. The details can be found in Ref. 12.

e. Inclusion of the Effect of Plasma Density and Temperature.

In previous sections, we discussed the calculation of atomic structure and processes for an isolated atom or ion - that is, without the effect of the plasma environment. This

is valid for very low density plasmas. As the plasma density increases, several additional effects due to screening shifts of energy levels (or lowering of ionization potential) and modification of wavefunctions and potentials for the ion embedded in high density plasmas have to be considered. We utilized the two-component finite temperature DFM to incorporate the effects of the plasma environment. Consider an ion (li-like Carbon, for example) embedded in a plasma in local thermodynamic equilibrium at a temperature T. The charged ion attracts the free electrons in the plasma, while pushing other charged ions away. Let $\rho(r)$ and $n(r)$ be the inhomogeneous ion and electron distribution in the plasma and $\bar{\rho}$ and $\bar{n}$ the corresponding mean densities. Over a sphere of radius R (the correlation sphere) surrounding the central ion, the electrical neutrality condition gives

$$\bar{z} \int_R \rho(\vec{r})\, d\vec{r} = z - \int_R n(\vec{r})\, d\vec{r} \qquad (13)$$

where $\bar{z}=z - n_b$, where n_b is the number of bound electrons of the ion. From first principles, the following set of coupled equations can be derived for electrons and ions in the plasma using the finite tempertaure two-component DFM:

$$\left[-\frac{1}{2}\nabla^2 + V^e(\vec{r})\right]\phi_i(\vec{r}) = \varepsilon_i \phi_i(\vec{r}) \qquad (14)$$

with

$$V^e(\vec{r}) = -\left[\frac{z}{r} + \int \frac{\bar{z}\,\rho(\vec{r})-n(\vec{r}')}{|\vec{r}-\vec{r}'|}\,d\vec{r}'\right] + V_{xc}^e(\vec{r}) - V_{xc}^e(\vec{R}) \tag{15}$$

$$n(r) = \sum_i f_b|\Phi_b(r)|^2 + \sum_{l=o}^{\infty} 2(2l+1)\int_o^{\infty} dk\; k^2\; f(k)|\Phi_{kl}(r)|^2 \tag{16}$$

In most plasma conditions, the ion distribution can be well represented by

$$\rho(r) = \bar{\rho}\; e^{\;-V^i/KT} \tag{17}$$

$$\text{with}\quad V^i(r) = \bar{z}\left[\frac{z}{r} + \int \frac{\bar{z}\,\rho(\vec{r})-n(\vec{r}')}{|\vec{r}-\vec{r}'|}\,\vec{d}r'\right] \tag{18}$$

In Eqs. (14) - (18), we note that the effective electron potential $V^e(r)$ is influenced both by the electron and the ion charge distributions: $n(r)$ and $\rho(r)$. The ion effective potential $V^i(r)$ is also influenced the same way. The electron density distribution in eq. (16) is determined from the contribution from the bound states Φ_b's as also from the continuum states $\Phi_{kl}(r)$ weighted by the integral occupation factors f_b's for bound electrons and the fermi distribution function f_k for free electrons.

The model outlined above incorporates several improvements over frequently used "average atom" models such as Thermi-Fermi. The present model is valid at any plasma density and temperature, i.e., both for weakly and strongly-coupled plasma conditions. The screening effect of both bound and free electrons are treated accurately in this model, unlike Thomas-Fermi. The many-body effects such as electron exchange and correlation are treated adequately. The electron degeneracy effect is included and realistic ion distribution is folded into the calculation and is made self-consistent to the electron distribution.

Debye-screened potentials have been used often to describe the plasma screening effects on atomic processes, such as photoionization. For comparison purposes, we carried out similar calculations for a few representative density and temperature using a simplified model. In this model, the long range part of the effective ionic potential was represented in the Debye-screened form, whereas the inner part of the ionic potential was calculated using the bound wavefunctions. Thus, the summation over a large number of continuum states and the corresponding iteration could be avoided and resulted in computational simplicity. The results are compared with the self-consistent DFM results. Let, us emphasize that the finite tenperature two-component DFM goes far beyond the Debye-screened model.

Debye screening is known to be inadequate in a wide range of plasma conditions whereas the DFM treats the screening effects in a fully non-linear self-consistent fashion and is therefore much more realistic and useful.

III. RESULTS

To see the usefulness of the time-dependent density functional method (TD-DFM) for generating photionization cross-sections, we first discuss the results for a few neutral atoms. In Fig. 1, results of computed photoionization cross-section for neutral Xenon is plotted as a function of photon energy near the 4d-threshold. The drastic difference between the TD-DFM(curve A) and the conventional IPA-model (Curve B) is clear. The IPA-model does not reproduce the experimental values[8] at all whereas the present TD-DFM model agrees very well with the experimental data over this entire range of photon energy from 5 to 10 Ryd., including the peak at about 7 Ryd. In that energy range, the IPA-cross section shows a rapid decrease - in contrast to the experimental data.

The primary physical reason for this difference in the two models arise from the polarization effect of the atom subject to the incident radiation. This collective effect is missing in the IPA-calculation. A large number of electrons forming the atom participate in the polarization process. The external field is screened in the energy range 5-6 Ryd (and again in the range 8.5 - 9.5 Ryd.), and is antiscreened in the intermediate 6-8 Ryd. range. The antiscreening effect produces a stronger effective field for the 4d-electron to photoionize, thereby enhancing the cross-section in the intermediate energy range as seen in Fig. 1.

The 3S-partial cross-section for Argon is shown in Fig. 2. The experimental data[9] in the range 30-65 eV are depicted by circles with error bars. The conventional IPA-calculation (curve A) again does not show the experimentally seen variation at all. The TD-DFM model reproduces the observed variation including the experimental Cooper minimum[1] at about 43 eV and is in good agreement with the measured cross-sections. The occurrence of the Cooper minimum is known to be due to the vanishing of the matrix element between bound and continuum states at that photon energy. In the TD-DFM model, the physical reason for the minimum is that the induced potential almost exactly cancels out the external field, reducing the effective field to almost zero.

The total cross-section for Argon atom as a function of the photon energy is plotted in Fig. 3, and compared with experimental data[11]. Comparison is also made of results obtained from Hartree-Fock (HF) length and velocity approximations[10]. The present TD-DFM model again best reproduces the experimental data. The HF-velocity approximation gives, for example, a cross-section twice as large at 40 eV whereas the HF-length result is six times larger than the experimental data at the same photon energy.

Good agreement with available experimental data is also obtained for Neon and Krypton by using the present TD-DFM model. This suggests that the TD-DFM model could be a reliable tool to generate photoionization and

photoabsorption data for multielectron ions of different Z. We, therefore, carried out the calculations for several ions of experimental interest for x-ray laser systems: H-like C, Li-like C, Li-like Ne, Ne-like Ar, Ne-like Se etc. For most of these ions, no experimental data is available and thus the data have to be provided by theoretical calculations.

In earlier discussion, it was pointed out that the collective effects of a large number of bound electrons is reponsible for the substantial difference between TD-DFM and Independent Particle Approximation (IPA) results. For highly stripped ions (such as the ones listed above), however, both models tend to produce similar results. For H-like C, for example, there is only 1 bound electron. The TD-DFM and the IPA-calculations therefore give the same result (Fig. 4). For Li-like Carbon with 3 bound electrons, the photoionization cross-sections are slightly different for the photon energy range 370-600 eV (Fig. 5). Li-like Neon also has three bound electrons. However, because of higher nuclear charge (Z=10), those electrons are tightly bound (more tightly than in neural Neon) and thus do not participate as effectively in the polarization process. Thus, the TD-DFM and IPA calculations lead to essentially the same results for Li-like Ne (Fig. 6(a) and 6(b)) and Ne-like Se (Fig. 8). For Ne-like Argon, the polarization process is somewhat more effective and leads to results that are somewhat different from IPA results over the photon energy range 450-600 eV (Fig 7). To see the variation of

the contribution of each electronic state to the total cross-section, the computed values for Li-like C, Li-like Ne and Ne-like Ar are given in Tables I-III.

The radiative decay rate of ions of specific configuration is another kind of atomic data necessary for atomic modeling for X-ray lasers. Once the wavefunctions and energy levels of the given multielectron ion has been generated from the atomic structure code, the radiative decay rate (or Einstein transition probability) can be calculated by evaluating the relevant matrix element[12]. In Table IV, the computed decay rates of some of the transitions for Neon-like Krypton is presented. (j-j) coupling has been used in these calculations. The ground state of Ne-like Krypton is $1S^2 2S^2 2p^6$ with total J=O. All energies in Table IV are given relative to the ground state energy of the ion which is taken to be Zero. We note from the table that the radiative decay rates vary substantially depending on the particular excited ionic state and the transition considered.

Next, we incorporated the effect of plasma density and temperature into our model and investigated the resulting modification of photoionization cross-sections of ions in plasmas. The plasma effects were studied first by using an approximate model in which the long range part of the ionic potential was taken in the form of Debye-screened potential (for the given plasma density and temperature). The inner part of the potential was constructed numerically using the

bound state wavefunctions as in Eq. (15). This avoids the large number of iterations with the continuum wavefunctions and thus leads to computational simplicity[13].

We applied this simplified model to H-like and Li-like Carbon ions in plasmas. The results are shown in Figures 9-12. The plasma densities considered are in the range 10^{22} - 10^{23} electrons/cm^3 and temperatures are in the range 30 - 50 eV. The corresponding Debye screening lengths are in the range of 2 - 5 au.

From Fig. 9, we see by comparing with isolated ion cross-sections, that the threshold for photoionization from 1s-level of H-like C shifts substantially (from 18 eV to about 15.2 eV) for Debye length λ_D=2 au. This is important in the context of calculation of photoionization rates, which is calculated by integrating the cross-section weighed by the electron distribution function (usually Maxwell-Boltzmann distribution) over the entire energy range. The calculated rates in the two cases would therefore be very different - as seen from Fig. 9.

In Fig. 10, the corresponding results of 2S photoionization cross-section for H-like C is plotted. Fig. 11 shows the 3d partial cross-sections of the same ion at two different plasma conditions (λ_D=5 and 2 au) and are compared with the isolated atom cross-section (curve A). The increasing shift of the ionization threshold with decreasing λ_D (i.e., with increasing density) is clear from the Figure 11. For Li-like Carbon, the 2S partial cross-

section at two different plasma conditions were computed using the simplified model and are shown in Fig. 12. Comparison with isolated ion cross-section shows substantial modification of photoionization cross-section at these densities and temperatures and significant shift of ionization threshold due to the effect of the surrounding plasma.

The full self-consistent calculation using the two-component DFM-model was also performed for Li-like Carbon in two different plasma conditions. The results are shown in Fig. 13 (λ_D=5 au). and Fig. 14 (λ_D=2 au). Curve B in both figures correspond to data obtained from the simplified model whereas curve C is the result of full self-consistent DFM calculation. The DFM model generates more accurate shifted energy levels; thus the shift of the threshold of 2S cross-section relative to the isolated ion threshold is more realistic in this model. In addition, the self-consistent DFM-model is seen to generate photoionization cross-sections that are substantially different from simplified model. The calculated rates resulting from these cross-sections also differ substantially.

IV. SUMMARY

Some of the atomic processes important for overall modeling of x-ray lasers have been investigated in this work, performed over the period June 1986 through July 1987. The atomic structure code for multielectron ions of arbitrary Z is of central importance in these computations. The code we have used for this purpose is based on local density functional method and provides a fast, efficient, accurate tool to generate energy levels, wave-functions, etc. for multielectron ions and atoms. Proper relativistic treatment is included in this code for high Z ions. We carried out computations of photoionization and photoexcitation cross-sections, radiative recombination, radiative decay rates for a variety of ions of different Z over a wide range of parameters of interest to X-ray lasers.

It is demonstrated that the time-dependent linear response method within the framework of density functional theory can provide reliable photoprocess (and recombination) data for various atoms and ions of experimental interest. This model is particularly useful in those situations where conventional independent particle models fail to provide accurate data. The mechanism of time-dependent polarization of the atom is seen to be important in describing the experimental results. As a practical point, the computer code based on the time-dependent model is fast and efficient, capable of generating a large number of data in a

short time (for example, cross-sections for 10 photon energies for a medium-z ion takes about 3 mins. of C.p.u. time on a Cray-XMP computer).

We also studied the effects of plasma density and temperature on atomic structure and processes such as photoionization and spontaneous transitions. The model and the computer code developed for this purpose is capable of treating screening effects in a fully non-linear fashion and thus goes beyond the often used Debye-screening model. The model represents a significant improvement over the "Average Atom" models (AAM) in a number of ways. The specific ionic configuration (with integral occupation) is maintained in our model-unlike AAM's. Both the bound and free electrons are treated fully quantum mechanically in this model (in contrast to AAM's such as Thomas-Fermi) and therefore, lead to more accurate electronic charge distribution and effective ionic potentials. The ion distribution in our model is treated self-consistently with the electron distribution via coupled equations. The present model is applicable in arbitrary plasma conditions and is therefore, useful in a wide range of densities and temperatures where models such as Thomas-Fermi or Debye-Huckel are known to be inadequate. The calculations done here show that, with increasing plasma density, the atomic data (such as photoionization cross-section) can be substantially modified from the isolated atomic values. The effects of plasma

density and temperature thus need to be included for realistic atomic modeling. The models presented here achieve that objective systematically.

The work performed have thus provided improved atomic modeling capability for X-ray laser plasmas and should be useful for application to different lasing schemes such as photopumping or radiative recombination. In addition, the models and the computer codes are useful tools for studies of radiative properties of hot plasmas of different densities, opacity calculations and plasma diagnostics.

V. ACKNOWLEDGEMENTS

I would like to express my sincere gratitude and appreciation of the support and encouragement of Dr. Robert Barker for this work. Thanks are also due to Dr. Milan Blaha of the University of Maryland for his help and for useful discussions.

VI. REFERENCES

1. U. Fano and J.W. Cooper, Rev. Mod. Phys. 40, 441 (1986).

2. M.J. Stott and E. Zaremba, Phys. Rev. A21, 12 (1980).

3. A. Zangwill and P. Soven, Phys. Rev. A21, 1561 (1980).

4. D. Liberman and A. Zangwill, Comput. Phys. Commun. 32, 75 (1984).

5. U. Gupta and A.K. Rajagopal, Review Article in Phys. Reports, 82, No. 6 (North Holland Publishing Co.) 1982.

6. U. Gupta, M. Blaha and J. Davis, J. Phys. B 17, 3617 (1984).

7. See, for example, R.D. Cowan and J. Ashkin, Phys. Rev. 105 (1957).

8. R. Hansel, G. Keitel, P. Schrieber and C. Kunz, Phys. Rev. 188, 1375 (1969).

9. K.H. Tan and C.E. Brion, J. Electron Spectros. 13, 77 (1978).

10. D.J. Kennedy and S.T. Manson, Phys. Rev. A5, 227 (1971)

11. J.A.R. Samson, Advan. Atom. Mod. Phys. 2, 178 (1966).

12. R.D. Cowan, "The Theory of Atomic Structure and Spectra," Univ. of Calif. Press (1981).

13. U. Gupta and M. Blaha, work presented at the Atomic, Molecular & Optical Physics Conference, Boston, Mass. May 18-20 (1987).

14. See, for example, W. Kohn and P. Vashista, Physics of Solids and Liquids, eds. S. Lundquist and N.H. March (Plenum, New York, 1983).

TABLE I

Li-Like C

Photon Energy (ev)	Electronic States	Photoionization Cross-Section (Megabarn)	
		IPA	TD-DFM
250	2S 1/2	0.0424	0.0370
300	2S 1/2	0.0280	0.0275
350	1S 1/2	0.5968	0.5969
	2S 1/2	0.0193	0.0190
	Total	0.6161	0.6159
400	1S 1/2	0.4354	0.4444
	2S 1/2	0.0141	0.0141
	Total	0.4495	0.4585
460	1S 1/2	0.3088	0.3203
	2S 1/2	0.0100	0.0101
	Total	0.3188	0.3304
500	1S 1/2	0.2499	0.2613
	2S 1/2	0.0081	0.0083
	Total	0.2S80	0.2695
550	1S 1/2	0.1954	0.2059
	2S 1/2	0.0065	0.0066
	Total	0.2019	0.212S
600	1S 1/2	0.1556	0.1650
	2S 1/2	0.0051	0.0053
	Total	0.1608	0.1703

TABLE II

Li-Like Ne

Photon Energy (ev)	Electronic States	Photoionization Cross-Section (Megabarn)	
		IPA	TD-DFM
230	2S 1/2	0.2108	0.2080
240	2S 1/2	0.1960	0.1932
260	2S 1/2	0.1673	0.1649
280	2S 1/2	0.1451	0.1430
300	2S 1/2	0.1265	0.1247
320	2S 1/2	0.1116	0.1099
340	2S 1/2	0.0986	0.0971
360	2S 1/2	0.0877	0.0863
1040	2S 1/2	0.0080	0.0099
1060	2S 1/2	0.0076	0.0074
1080	2S 1/2	0.0073	0.0082
2000	1S 1/2	0.0379	0.0395
	2S 1/2	0.0015	0.0016
	Total	0.0395	0.0411
2040	1S 1/2	0.0359	0.0375
	2S 1/2	0.0014	0.0015
	Total	0.0373	0.0390

TABLE III

Ne-Like Ar

Photon Energy (ev)	Electronic States	Photoionization Cross-Section (Megabarn)	
		IPA	TD-DFM
395	2p 3/2	1.0061	0.9481
400	2p 1/2	0.4984	0.5060
	2p 3/2	0.9905	1.0065
	Total	1.4889	1.5125
420	2p 1/2	0.4339	0.4465
	2p 3/2	0.8593	0.8855
	Total	1.2931	1.3321
440	2p 1/2	0.3952	0.4183
	2p 3/2	0.7807	0.8273
	Total	1.1759	1.2457
460	2p 1/2	0.3509	0.3774
	2p 3/2	0.6938	0.7468
	Total	1.0447	1.1243
480	2S 1/2	0.1981	0.2073
	2p 1/2	0.3188	0.3471
	2p 3/2	0.6297	0.6863
	Total	1.1466	1.2407
500	2S 1/2	0.1901	0.1995
	2p 1/2	0.2867	0.3159
	2p 3/2	0.5656	0.6239
	Total	1.0424	1.1393
520	2S 1/2	0.1769	0.1863
	2p 1/2	0.2604	0.2893
	2p 3/2	0.5139	0.5717
	Total	0.9512	1.0473
540	2S 1/2	0.1682	0.1776
	2p 1/2	0.2368	0.2657
	2p 3/2	0.4668	0.5243
	Total	0.8719	0.9676
560	2S 1/2	0.1497	0.1589
	2p 1/2	0.1971	0.2240
	2p 3/2	0.3884	0.4419
	Total	0.7351	0.8247
600	2S 1/2	0.1422	0.1513
	2p 1/2	0.1804	0.2063
	2p 3/2	0.3553	0.4068
	Total	0.6779	0.7643

TABLE IV

Neon-Like Krypton

Initial State	Energy* (ev)	Final State	Energy* (ev)	Radiative Decay Rate**
$2p^5 3s(3/2,1/2)J=1$	1652.94	$2p^6(0,0)J=0$	0.00	5.04E+12
$2p^5 3d(3/2,3/2)J=1$	1782.71	$2p^6(0,0)J=0$	0.00	2.58E+11
$2p^5 3p(3/2,1/2)J=1$	1701.40	$2p^5 3s$ $(3/2,1/2)J=2$	1649.75	7.87E+09
$2p^5 4p$	2282.36	$2p^5 3s$ $(3/2,1/2)J=2$	1649.95	6.97E+11
$2p^5 4f$	2324.58	$2p^5 3s$ $(3/2,1/2)J=2$	1649.95	9.24E+07
$2p^5 4s$	2237.98	$2p^5 3p$ $(3/2,1/2)J=1$	1701.40	2.54E+11
$2p^5 4d$	2310.79	$2p^5 3p$ $(3/2,1/2)J=1$	1701.40	3.27E+11
$2p^5 3s(1/2,1/2)J=1$	1707.72	$2p^5 3p$ $(3/2,1/2)J=2$	1704.20	2.03E+02
$2p^5 3d(3/2,3/2)J=1$	1781.71	$2p^5 3p$ $(3/2,1/2)J=2$	1704.20	2.54E+09
$2p^5 4p$	2282.36	$2p^5 3d$ $(3/2,3/2)J=0$	1780.34	6.84E+09
$2p^5 4f$	2324.58	$2p^5 3d$ $(3/2,3/2)J=0$	1780.34	1.36E+11
$2p^5 4d$	2310.79	$2p^5 4p$	2282.36	5.68E+09

*All energies are measured relative to the ground state: $2p^6(0,0)J=0$. The numbers in parenthesis are the j-value of the parent ion and that of the outer electron.

** (Sec^{-1})

Figure 1

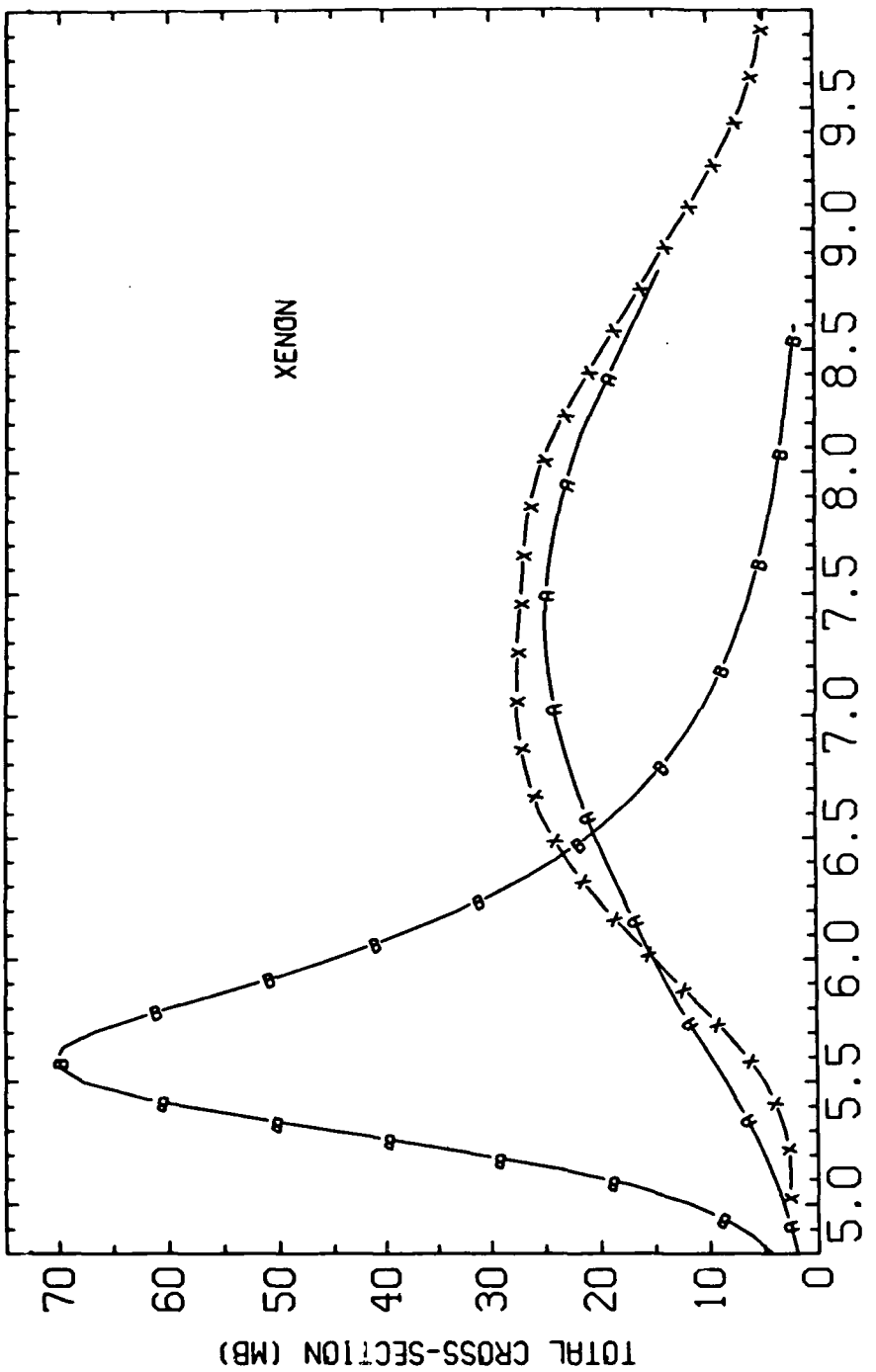

TOTAL PHOTOIONIZATION CROSS-SECTION OF NEUTRAL XENON NEAR 4D THRESHOLD. CURVE A: TIME DEPENDENT DENSITY FUNCTIONAL CALCULATION. CURVE B: INDEPENDENT PARTICLE MODEL. EXPERIMENTAL DATA FROM R. HANSEL ET. AL., PHYS. REV. 188, 1375 (1969)

Figure 2

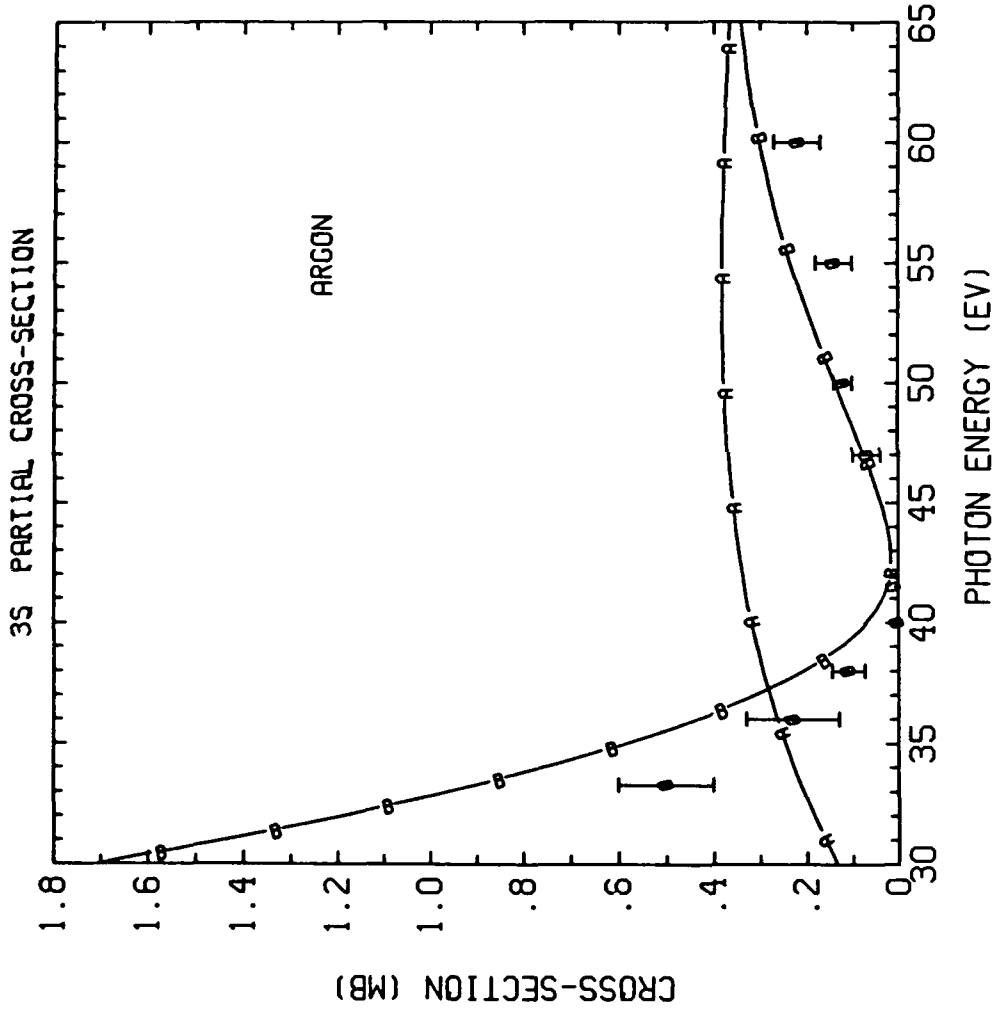

CURVE A: INDEPENDENT PARTICLE MODEL.

CURVE B: TIME-DEPENDENT DENSITY FUNCTIONAL CALCULATION.

DATA FROM K. TAN & C. BRION, J. ELECTRON SPECTROS. 13, 77(1978).

Figure 3

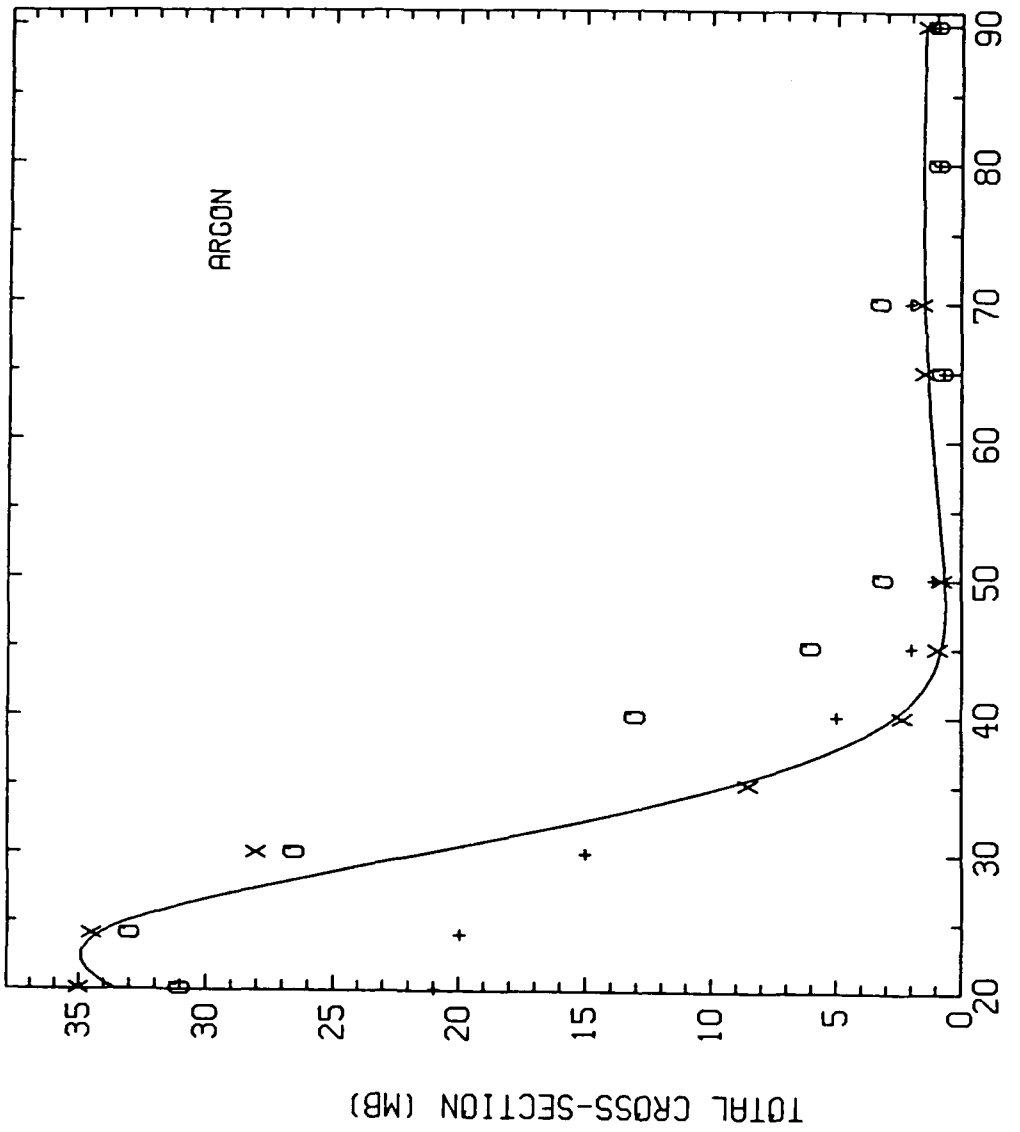

SOLID CURVE: TIME-DEPENDENT DENSITY FUNCTIONAL CALCULATION.
X: EXPERIMANTAL DATA FROM J.A.R.SAMSON, ADVAN. ATOM. MOL.
PHYS. 2, 178(1966). +: HARTREE-FOCK (VELOCITY APPROX.) AND
O: HARTREE-FOCK (LENGTH APPROX.) BY KENNEDY & MANSON,
PHYS. REV. A 5, 227(1972).

Figure 4

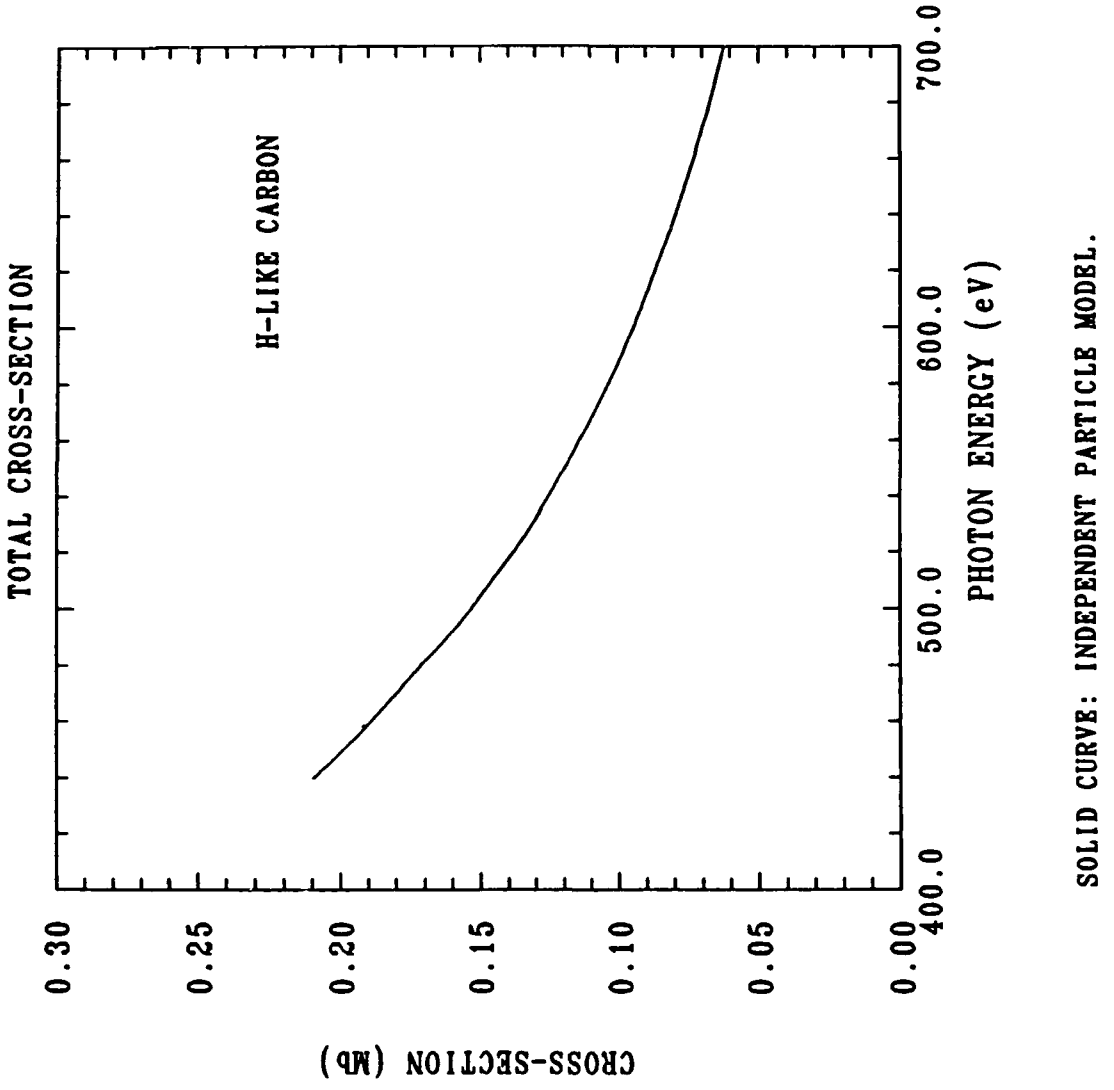
TOTAL CROSS-SECTION
H-LIKE CARBON
CROSS-SECTION (Mb)
0.30
0.25
0.20
0.15
0.10
0.05
0.00
400.0
500.0
600.0
700.0
PHOTON ENERGY (eV)
SOLID CURVE: INDEPENDENT PARTICLE MODEL.

Figure 5

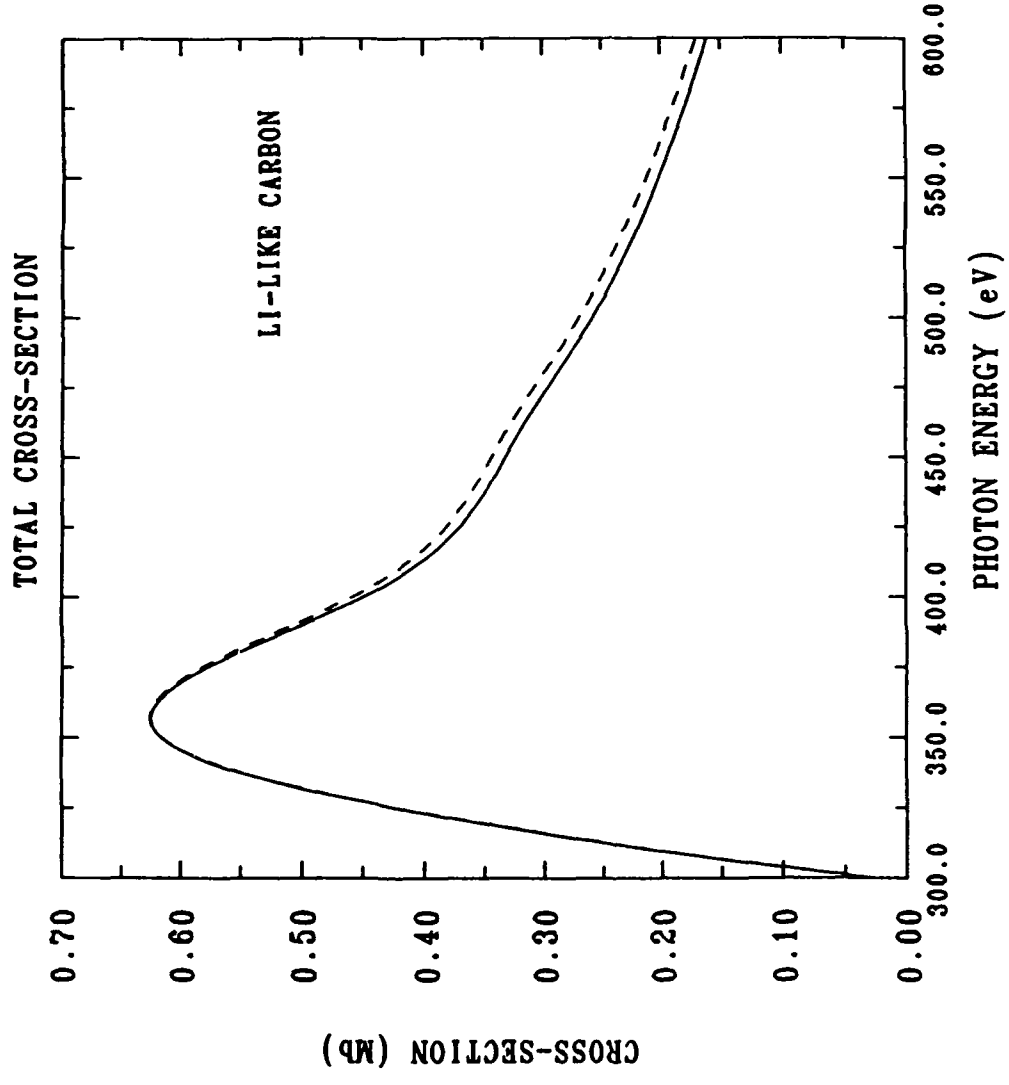

SOLID CURVE: INDEPENDENT PARTICLE MODEL.
DASHED CURVE: TIME-DEPENDENT DENSITY FUNCTIONAL CALCULATION.

Figure 6(a)

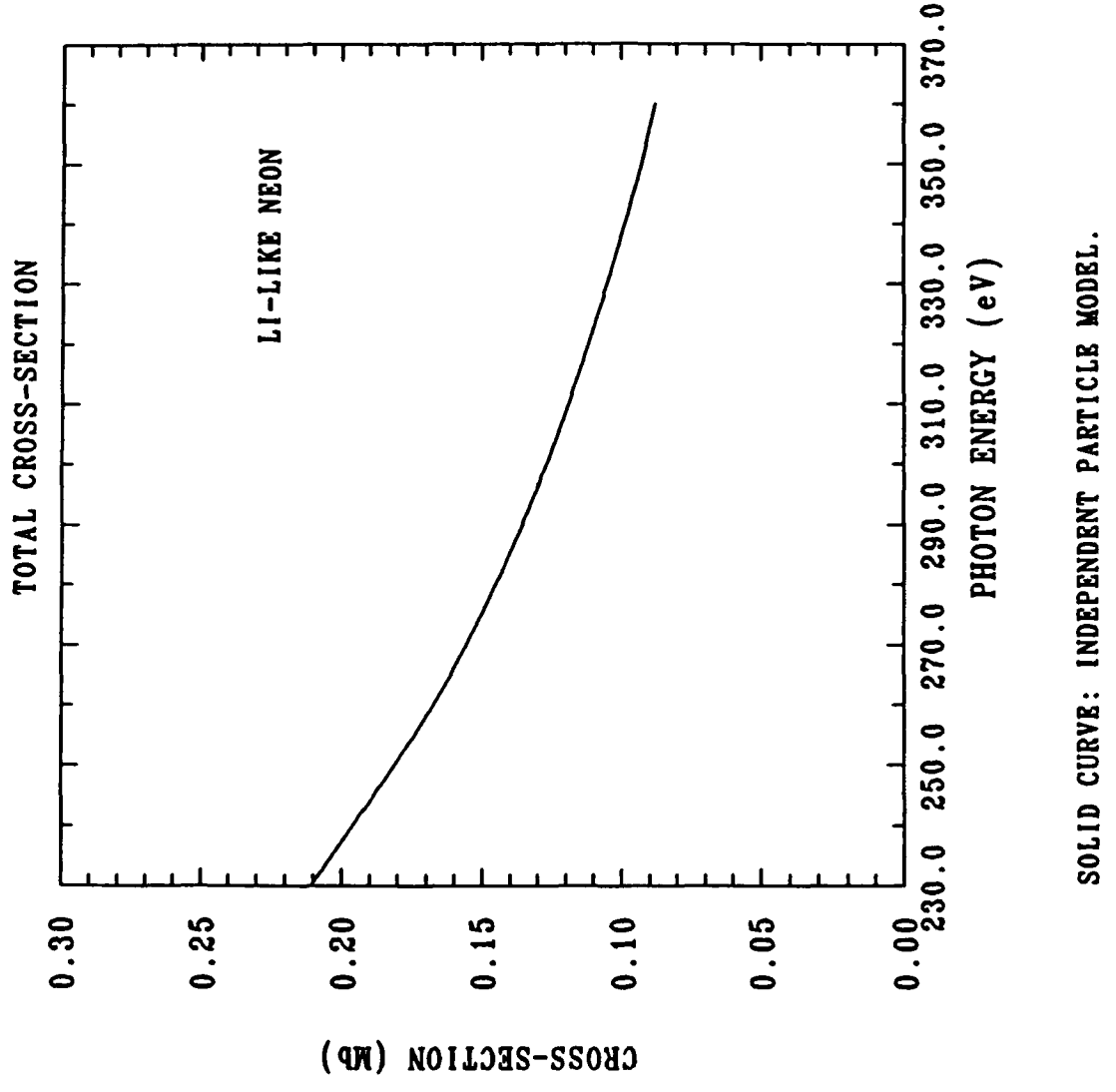
TOTAL CROSS-SECTION
LI-LIKE NEON
CROSS-SECTION (Mb)
0.30
0.25
0.20
0.15
0.10
0.05
0.00
230.0
250.0
270.0
290.0
310.0
330.0
350.0
370.0
PHOTON ENERGY (eV)
SOLID CURVE: INDEPENDENT PARTICLE MODEL.

Figure 6(b)

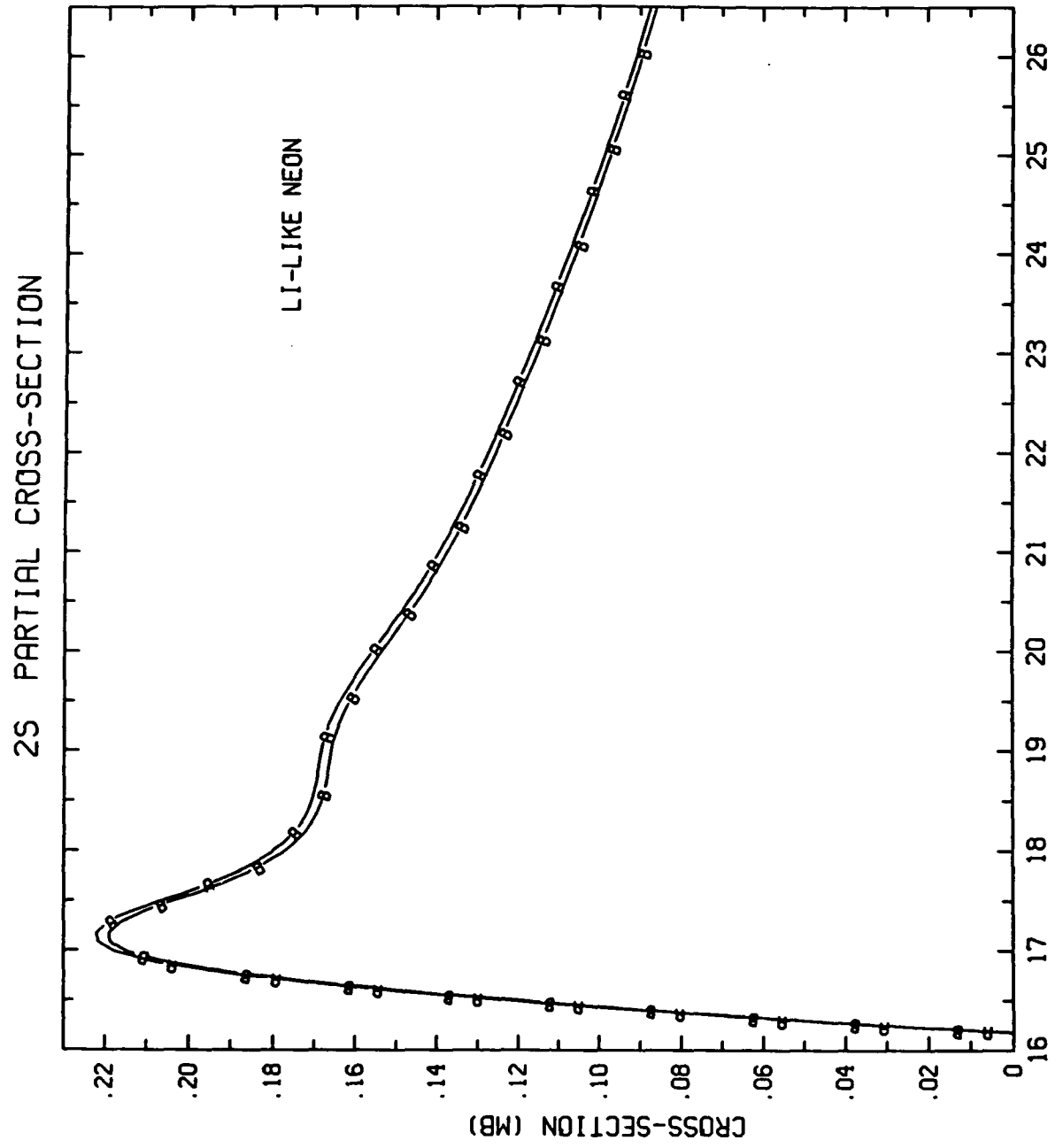

CURVE A: INDEPENDENT PARTICLE MODEL. CURVE B: TIME-DEPENDENT DENSITY FUNCTIONAL CALCULATION.

Figure 7

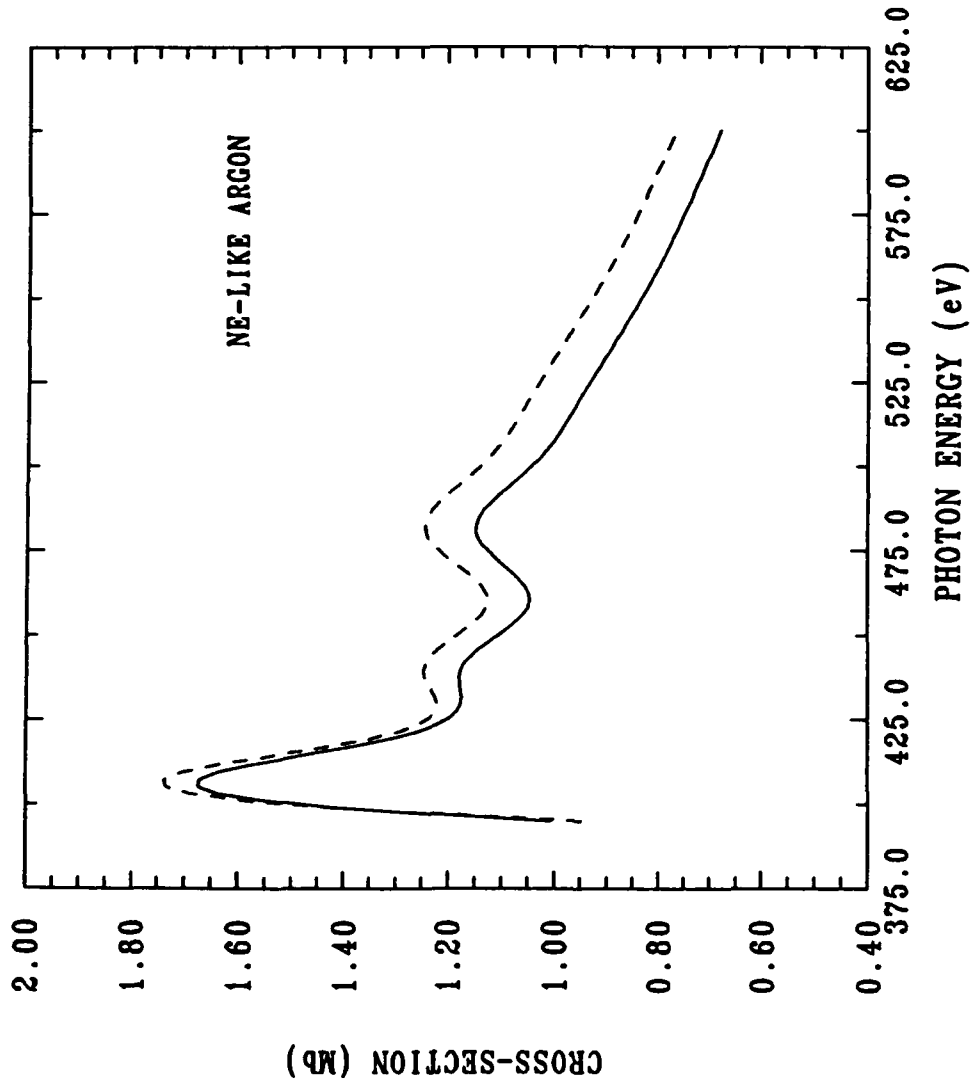

SOLID CURVE: INDEPENDENT PARTICLE MODEL.
DASHED CURVE: TIME-DEPENDENT DENSITY FUNCTIONAL CALCULATION.

Figure 8

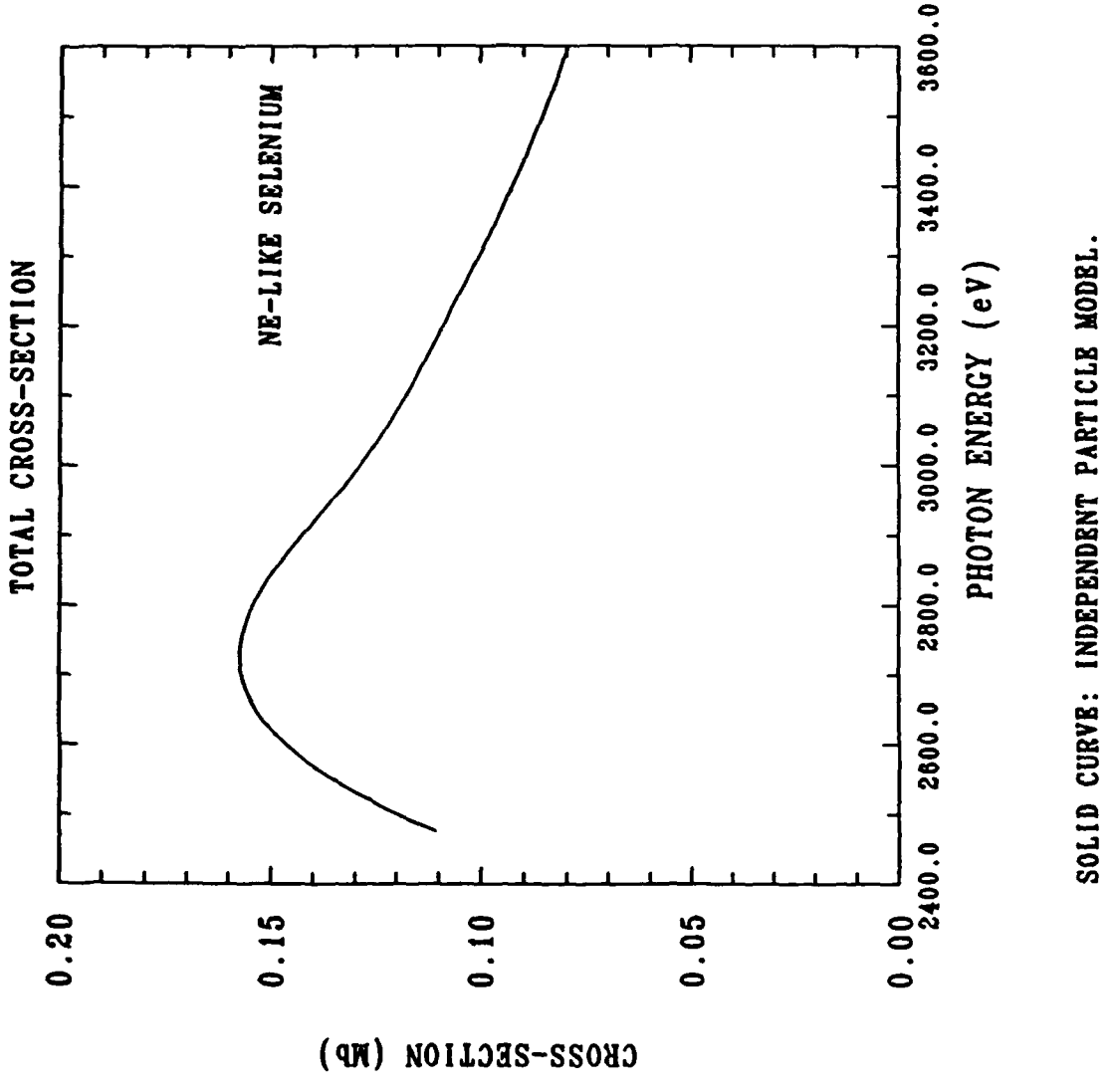

SOLID CURVE: INDEPENDENT PARTICLE MODEL.

Figure 9

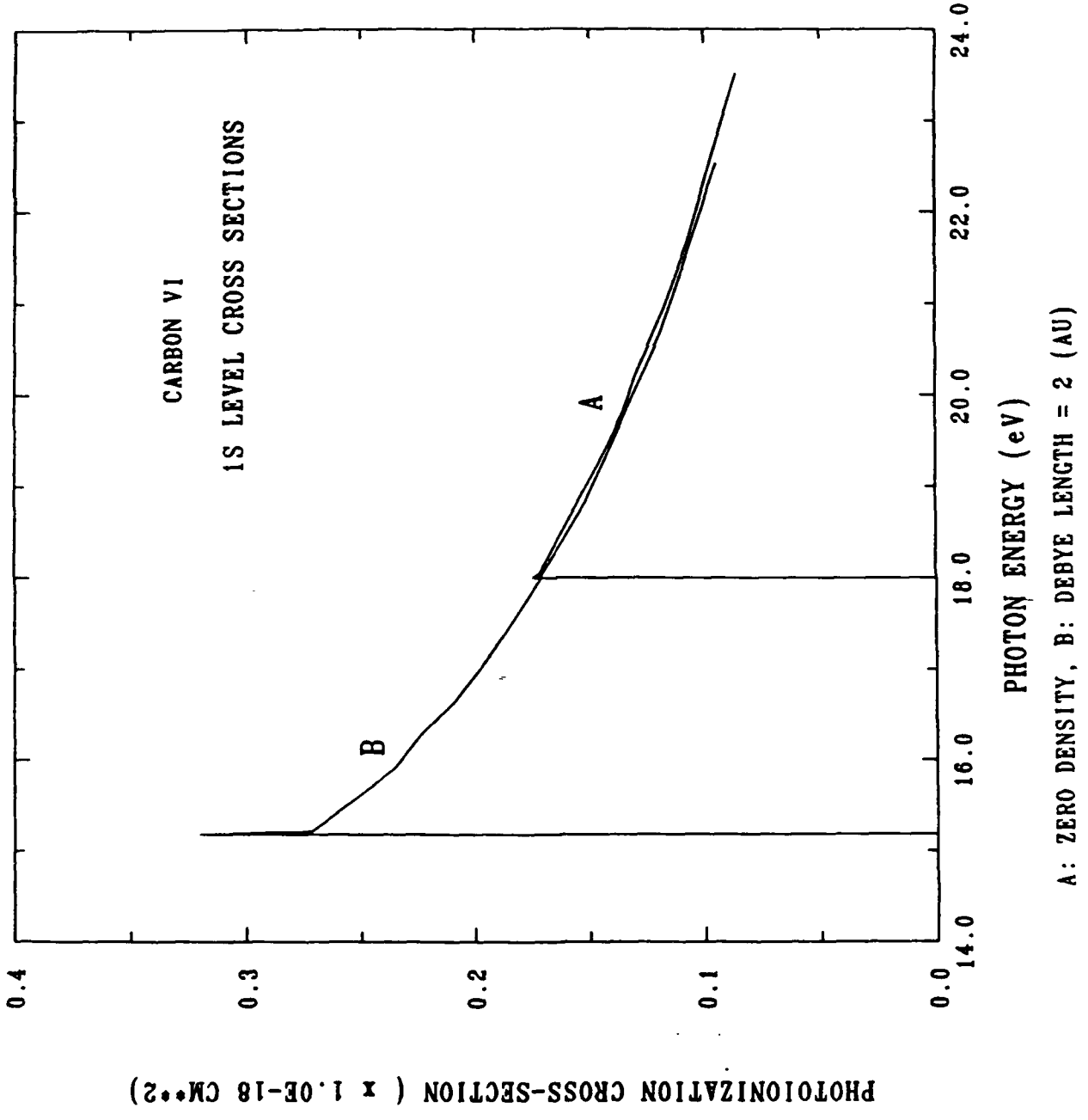
CARBON VI
1S LEVEL CROSS SECTIONS
A
B
0.4
0.3
0.2
0.1
0.0
14.0
16.0
18.0
20.0
22.0
24.0
PHOTOIONIZATION CROSS-SECTION (x 1.0E-18 CM**2)
PHOTON ENERGY (eV)
A: ZERO DENSITY, B: DEBYE LENGTH = 2 (AU)

Figure 10

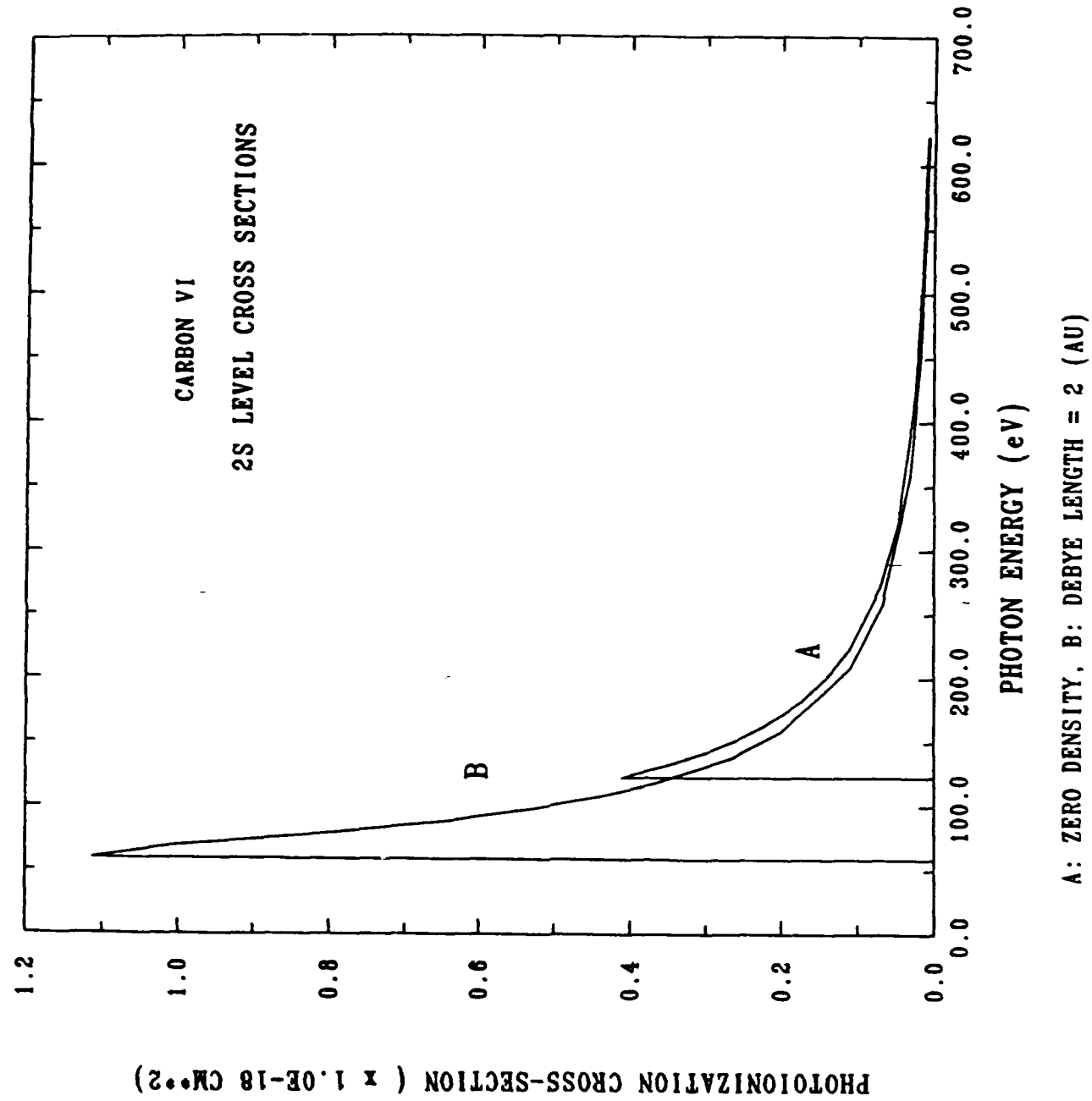
CARBON VI
2S LEVEL CROSS SECTIONS
A
B
PHOTOIONIZATION CROSS-SECTION (x 1.0E-18 CM**2)
PHOTON ENERGY (eV)
A: ZERO DENSITY, B: DEBYE LENGTH = 2 (AU)
0.0
0.2
0.4
0.6
0.8
1.0
1.2
100.0
200.0
300.0
400.0
500.0
600.0
700.0

Figure 11

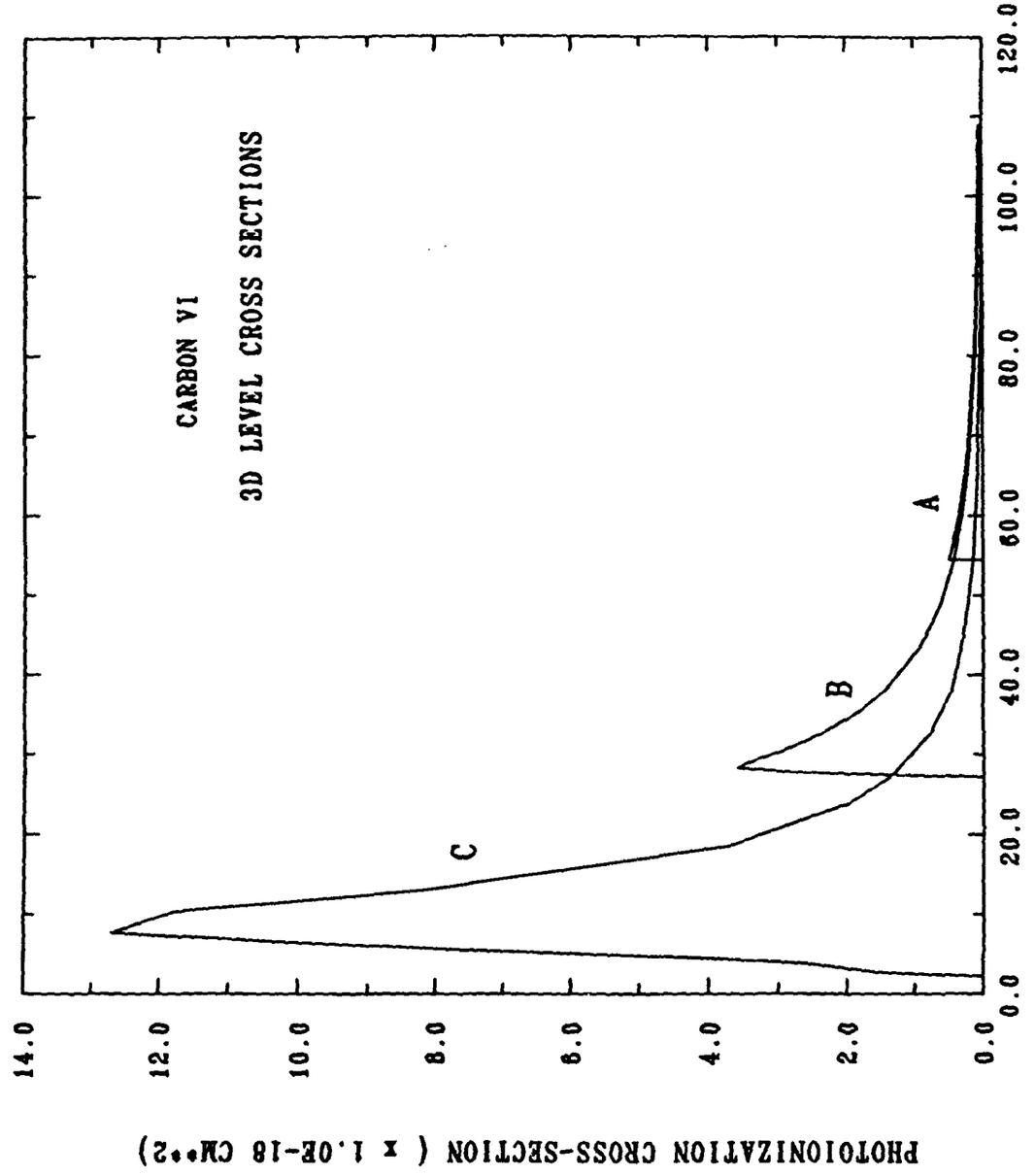

A: ZERO DENSITY, B: DEBYE LENGTH = 5 (AU)
C: DEBYE LENGTH = 2 (AU).

Figure 12

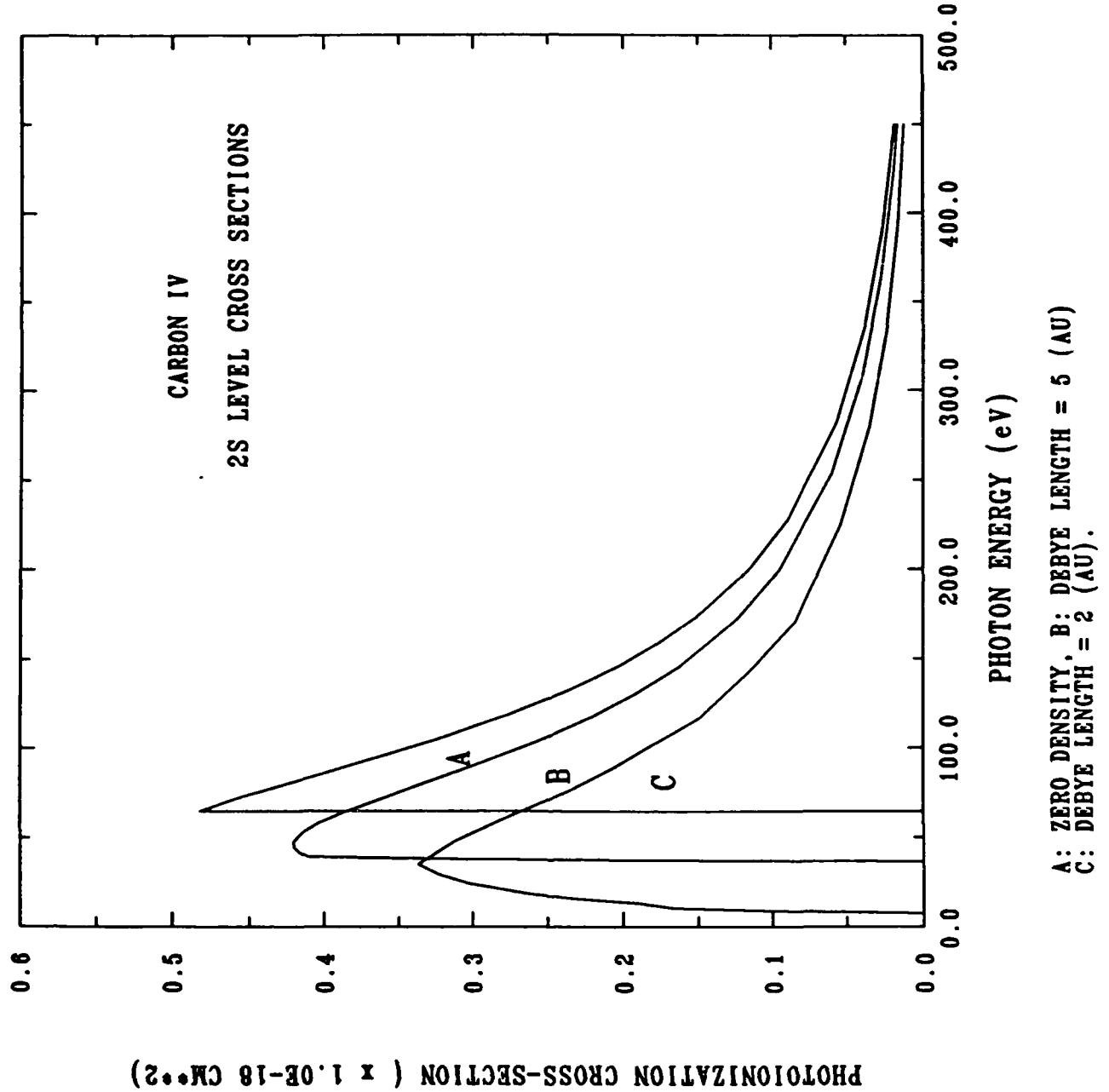
CARBON IV
2S LEVEL CROSS SECTIONS
A
B
C
0.0
0.1
0.2
0.3
0.4
0.5
0.6
100.0
200.0
300.0
400.0
500.0
PHOTON ENERGY (eV)
PHOTOIONIZATION CROSS-SECTION (x 1.0E-18 CM**2)
A: ZERO DENSITY, B: DEBYE LENGTH = 5 (AU)
C: DEBYE LENGTH = 2 (AU).

Figure 13

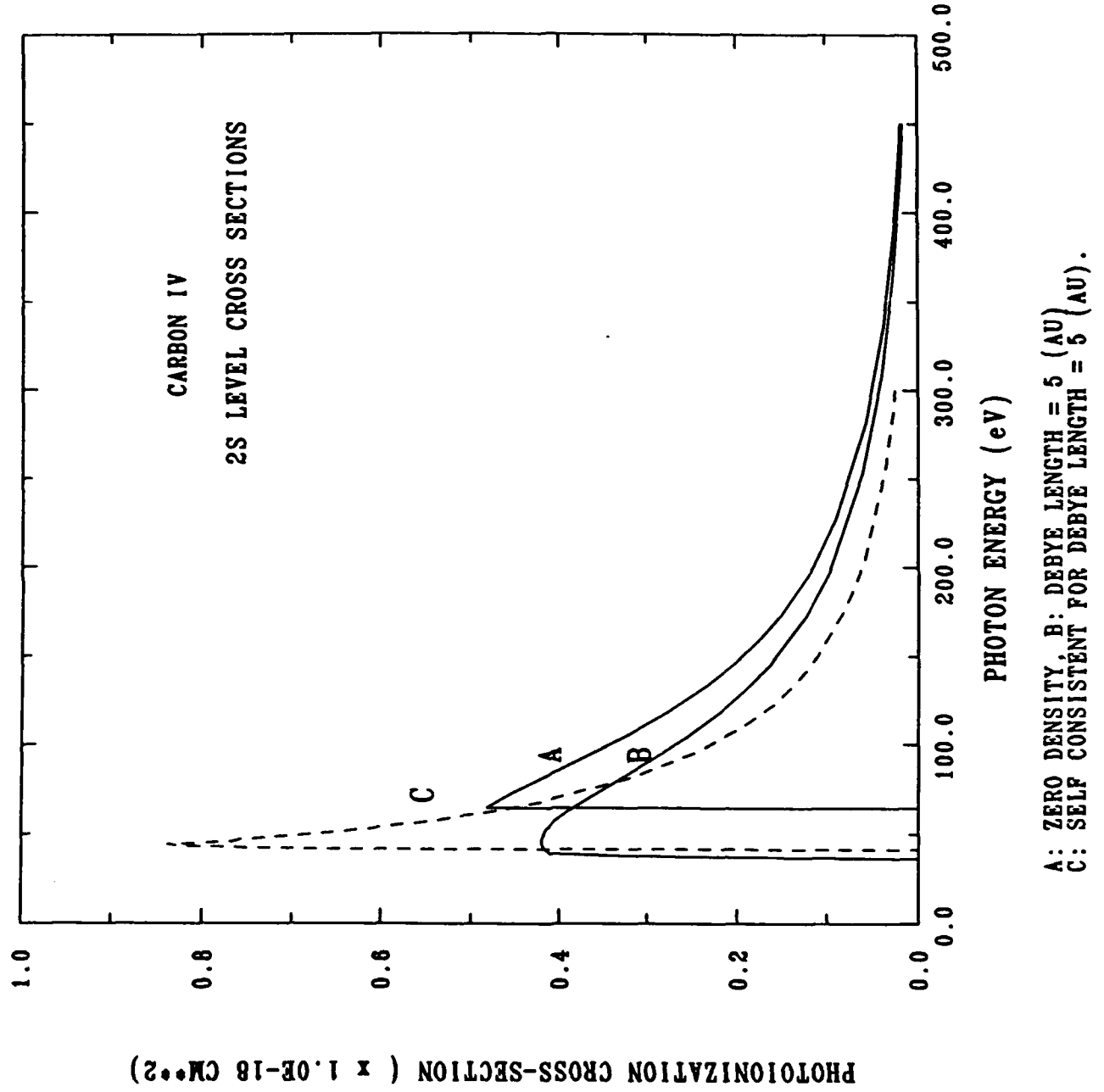
CARBON IV
2S LEVEL CROSS SECTIONS
A
B
C
0.0
0.2
0.4
0.6
0.8
1.0
0.0
100.0
200.0
300.0
400.0
500.0
PHOTOIONIZATION CROSS-SECTION (x 1.0E-18 CM**2)
PHOTON ENERGY (eV)
A: ZERO DENSITY, B: DEBYE LENGTH = 5 (AU)
C: SELF CONSISTENT FOR DEBYE LENGTH = 5 (AU).

Figure 14

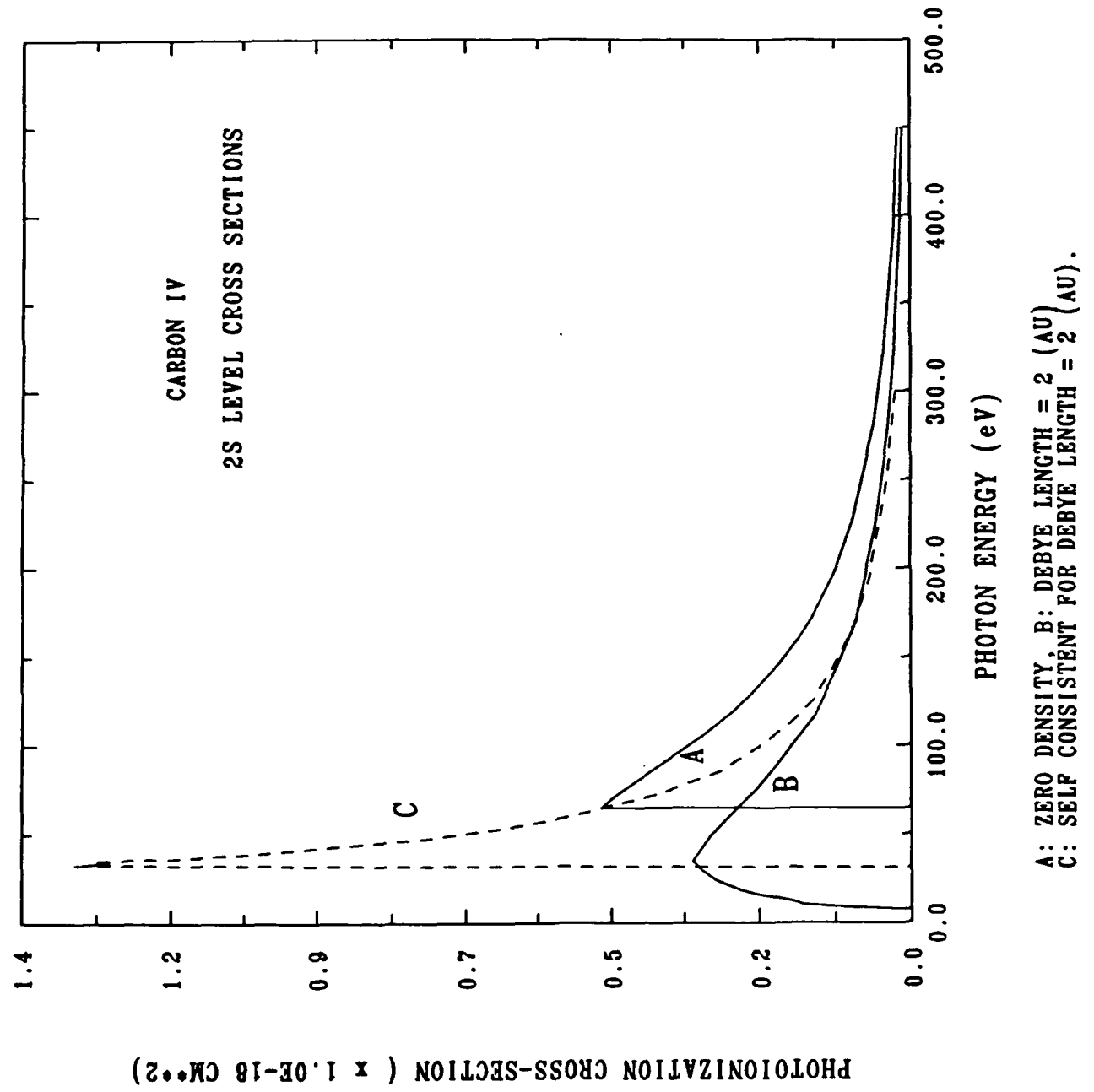
CARBON IV
2S LEVEL CROSS SECTIONS
PHOTOIONIZATION CROSS-SECTION (x 1.0E-18 CM**2)
PHOTON ENERGY (eV)
1.4
1.2
0.9
0.7
0.5
0.2
0.0
0.0
100.0
200.0
300.0
400.0
500.0
A
B
C
A: ZERO DENSITY, B: DEBYE LENGTH = 2 (AU)
C: SELF CONSISTENT FOR DEBYE LENGTH = 2 (AU).

PART II

MODELING OF ATOMIC PROCESSES

FOR

X-RAY LASER PLASMAS

TABLE OF CONTENTS

I. INTRODUCTION

Electron collisional excitation is one of the important mechanisms through which population inversion of ionic energy levels leading to lasing in the soft x-ray region can be achieved. Several research groups had suggested schemes based on electron collisional excitation processes as the pumping mechanism[1-6]. Recent experimental observation at Livermore[7-8] of 3p-3s amplification in Ne-like Selenium at 206 and 209 Å using a laser driven exploding foil target demonstrates the usefulness of electron collisional excitation (as also the radiative recombination processes) as a pumping mechanism leading to lasing.

Aside from the application to x-ray lasers, electron collisional ionization and excitation processes are among the various important atomic processes in overall modeling of radiative properties of plasmas in a wide range of experimental conditions. In the non local thermodynamic equilibrium (NLTE) conditions, which frequently occur in plasmas, the detailed rate equation approach to modeling requires a large variety of atomic data. Electron collisional ionization and excitation cross-sections and rates (along with other bound-bound, bound-free and free-free processes such as photoionization, photoexcitation, radiative recombination and decay, etc.) are necessary inputs to these calculations. Accurate calculations of electron collisional ionization and excitation processes are therefore needed for the different modeling mentioned above. Also, even though some experimental data for scattering cross-sections exist for certain atoms and ions; there is a lack of experimental data for many different types of atoms and ions over a wide range of energy. Thus, the required data have to be provided by theoretical calculations.

In theoretical calculations of electron scattering cross-sections, semi-classical impact (SCI) approximation has been used in some cases to generate the data[9]. The SCI-method, however,

turns out to be inadequate in many cases. Firstly, the SCI-method requires the choice of an impact parameter cutoff for which there is no absolute prescription. This arbitrariness can lead to certain errors. The method itself is restricted to dipole allowed excitations. Also, for large line strengths, the assumption of weak coupling in SCI-method is inadequate. Improving the first Born approximation requires a partial wave analysis.

In view of these, it is necessary to employ methods such as the Distorted Wave with exchange (DWEX)[10] or the Close Coupling (CC) scheme[11] to carry out the calculations of electron collisional cross-sections. The relative merits of these methods will be clear from the outline of these schemes presented in the next section. In general, the close coupling method can provide data of high accuracy; although in many cases, the DWEX can generate data within a few percent of the close coupling results.

For this 6-month project (August 1987 - February 1988), we carried out computation of electron impact ionization and excitation cross-sections and rate coefficients for different ions of interest over a wide range of incident electron energy. Most of the calculations were performed using the Distorted Wave with exchange (DWEX) method - since this provides a speedy and fairly accurate tool for these calculations. The outline for computational procedure and relative merits of the DWEX and close-coupling methods are given in Section II. Some selected results for collisional ionization cross-sections, rate coefficients for different electronic transitions for ions of interest are presented in Section III. The present work forms a useful component for the overall atomic modeling capability for x-ray laser and laboratory plasmas.

II. THE METHOD OF CALCULATION

In this section, we will briefly outline the Distorted Wave and the Close-coupling methods of electron-atom (or ion) scattering. The Close-coupling (CC) method is computationally more complex and requires substantial computer time. Use of good target wave functions are essential for accuracy in calculation. A short discussion of target wavefunctions is therefore, included.

A. The Close Coupling Method

Consider an atomic system containing (N+1) electrons. The electron coordinates are $\bar{x}_n = (\bar{r}_n, \sigma_n)$, n=1 to (N+1), where $\bar{r}_n$ is a position vector and ρ_n is a spin coordinate. States of the N electron system are referred to as "target" states.

$$\text{Let } \chi\left(\Gamma_i\ S_i\ L_i\ M_{si} M_{Li}\ \Pi_i \mid \bar{x}_n^{-1}\right) \text{ be a target state}$$

depending on all coordinates except $\bar{x}_n$. The angular momenta of the target are specified by S_i L_i M_{si} M_{Li} and Π_i is the parity of the target. Let the set of quantum numbers Γ_i S_i L_i l_i be collectively denoted by i. We will refer to i as the channel index. In the close-coupling approximation, the complete wavefunction is taken to be

$$\Psi = A \sum_{i=1}^{l} \chi_i \left(r_n^{-1}\right) \left(\frac{1}{r_n}\right) F_i(r_n) + \sum_{j=1}^{J} \Phi_j\ c_j, \qquad (1)$$

where A is the antisymmetrization operator, Φ_j's are the square integrable functions for the entire system, the radial functions $F_i(r)$ and the coefficients c_j's are fully optimized. The $F_i(r)$'s are made orthogonal to all radial functions with $l=l_i$ used to construct the states χ_i and Φ_i. The set of functions Φ_j must be such that the imposition of these orthogonality conditions does not imply a constraint on the total wavefunction Ψ.

Let E be the total energy, E_i the energy for the target state i and ϵ_i the energy of the added electron. Then

$$E = E_i + \epsilon_i \tag{2}$$

At energies giving bound states for the whole system we have $\epsilon_i < 0$ for all i and the radial functions $F_i(r)$ go to zero exponentially in the limit $r \to \infty$. The wavefunctions Ψ for bound states are normalized to unity. The collision states are such that $\epsilon_i > 0$ for some values of i. Channel i is said to be open if $\epsilon_i > 0$ and closed if $\epsilon_i < 0$. Let the E_i be ordered such that $E_1 < E_2 < \ldots < E_I$. For a given E, we have I_o open channels and

$$\begin{aligned} \epsilon_i &> 0 \quad \text{for } i = 1 \text{ to } I_o \\ \epsilon_i &< 0 \quad \text{for } i = (I_o+1) \text{ to } I. \end{aligned} \tag{3}$$

For numerical work, we first calculate real functions $F_{ii'}(r)$ satisfying the boundary conditions

$$\begin{aligned} F_{ii'}(r) &\underset{r\to\infty}{\sim} s_i(r)\,\delta(i,i') + c_i(r)\,\tilde{K}(i,i'), \quad \text{for } i = 1 \text{ to } I_o \\ F_{ii'}(r) &\underset{r\to 0}{\sim} 0 \qquad\qquad\qquad\qquad\quad \text{for } i = (I_o+1) \text{ to } I, \end{aligned} \tag{4}$$

with $i'=1$ to I_o. The functions $S_i(r)$ and $C_i(r)$ are Coulomb functions and $\tilde{K}$ is the reactance matrix.

Further, construct the Coulomb functions

$$\Phi^{\pm} = c \pm is \tag{5}$$

with the asymptotic forms

$$\Phi^{\pm} \sim (\pi k)^{-1/2} \exp(\pm i\zeta) \tag{6}$$

with

$$\zeta = kr - \frac{1}{2} l\pi + \left(\frac{z}{k}\right) \ln(2kr) + \arg \Gamma(l+1 - iz/k) \tag{7}$$

where z is the charge on the target system, z = (Z-N) with Z as the nuclear charge.

The cross-sections can be determined from $\tilde{S}$-matrix which is related to $\Phi^{\pm}$ asymptotically as:

$$F_{ii'}(r) \sim \frac{1}{2} \left\{ \Phi_i^-(r)\, \delta(i,i') - \Phi_i^+(r) \tilde{S}(i,i') \right\}$$
$$\text{for } i = 1 \text{ to } I_o \tag{8}$$
$$F_{ii'}(r) \sim 0$$
$$\text{for } i = (I_o+1) \text{ to } I.$$

The collision strengths are usually expressed in terms of the square of the appropriate $\tilde{T}$-matrix elements and therefore to the $\tilde{S}$-matrix elements.

B. Distorted Wave Method

It is well known that the DW approximation is appropriate whenever there are a sufficiently large number of angular momentum states contributing to the cross-section. For highly stripped ions, this method can be used for all angular momentum contributions.

Let Ψ^t be the trial wavefunction of the total system with the asymptotic form

$$\Psi^t \rightarrow k_\Gamma^{-1/2}\Phi_\Gamma\, r_j^{-1} \sin(\chi_j + \tau_\Gamma)$$
$$+ \sum_{\Gamma'} \rho(\Gamma,\Gamma')\, k_{\Gamma'}^{-1/2}\Phi_{\Gamma'}\, r_j^{-1}\cos(\chi_j + \tau_{\Gamma'}) \tag{9}$$

Where k_Γ^2 is the energy in Rydbergs of the incident electron in the channel $\Gamma \equiv \alpha L_\alpha S_\alpha l_\alpha L^T S^T$ with l_α the orbital angular momentum of the colliding electron, L^T and S^T are orbital and spin angular momenta of the total system (atom + colliding electron), L_α and S_α the orbital and spin angular momentum of the colliding electron. $\rho(\Gamma,\Gamma')$ are the elements of the $\tilde{\rho}$-matrix which in turn are related to $\tilde{S}$-matrix of scattering theory. The matrix element $\rho(\Gamma,\Gamma')$ of the trial matrix ρ^t is given by

$$\rho(\Gamma,\Gamma') = \rho^t(\Gamma,\Gamma') - 2 < \Psi_\Gamma^t \mid H-E \mid \Psi_{\Gamma'}^t, > \tag{10}$$

where H is the Hamiltonian of the total system and E is the total energy.

The trial wavefunctions Ψ_Γ^t are constructed from one-electron orbital wavefunctions of the form

$$\Phi_{nlm} = Y_{lm}(\Theta,\Phi)\, P_{nl}(r)/r \tag{11}$$

for atomic electrons and

$$\Phi_{klm} = Y_{lm}(\Theta,\Phi)\, F_{kl}(r)/r \tag{12}$$

for the colliding electron. Radial functions P_{nl} should satisfy the corresponding Hartree-Fock equations for atomic states $\alpha L_\alpha S_\alpha$ or $\beta L_\beta S_\beta$. F_{kl} is a solution of the equation

$$\left[\frac{d^2}{dr^2} - \frac{l(l+1)}{r^2} + \frac{2Z_n}{r} - 2\,V(r) + k_\Gamma^2\right] F_{kl} = 0 \tag{13}$$

with the asymptotic form

$$F_{kl} \rightarrow k_\Gamma^{-1/2} \sin(\chi + \tau_\Gamma) \qquad (14)$$

where Z_n is the nuclear charge and V(r) is given by

$$V(r) = \frac{1}{r} \int_0^r \sum_i P_i^2(y)\, dy + \int_r^\infty \frac{1}{y} \sum_i P_i^2(y) dy \qquad (15)$$

with P_i's the radial functions of all atomic electrons associated with the channel Γ. The orthogonality of radial functions are incorporated in the procedure via the method of Lagrange multipliers. The atomic potential in eq.(15) is supplemented by the exchange and correlation potential as in the Slater's $\chi\alpha$-method[12]. In our calculation, the one-electron orbital wavefunctions are generated self-consistently by iterative procedure by using the atomic structure code developed in our earlier work[13].

C. The Target Functions

Use of good target wavefunctions are essential for accurate scattering calculations. Radial functions of two types can be employed; spectroscopic orbitals, nl, of the type which one would have in a simple independent particle model and correlation orbitals $\bar{n}l$, which are included to give better accuracy.

In close coupling calculations it is convenient to use the same orthonormal sets of orbitals for all of the functions χ_i and Φ_j. For illustration, consider the simple case of He-like targets for which one may wish to include target states:

$$1s\ 2p\ {}^1P^0 \text{ and } 1s\ 2p\ {}^3P^0.$$

Complete optimization of the orbitals using the Hartree-Fock method will give two radial functions: $(2p)_1$, for $^1P^0$ and $(2p)_3$ for $^3P^0$, which may be significantly different. One procedure is to use one spectroscopic function 2p and one correlation function $\overline{3}p$ and to take the target functions to be linear combinations of the two configurations 1s 2p and 1s $\overline{3}p$. With a suitable choice of the ^2P and $\overline{3}p$ functions, this can be equivalent to the use of the fully optimized functions $(2p)_1$ and $(2p)_3$. Further configurations can be added if better accuracy is required. The radial functions are calculated numerically from the Schrodinger equation with an effective atomic potential. The effective atomic potential in our calculations[15] consists of the nuclear term, the electrostatic Hartree term plus the exchange-correlation potential that accounts for the interaction of the many electrons forming the atom or ion.

III. RESULTS

The Distorted Wave with Exchange method was employed to compute the electron collision strengths and cross-sections for Li-like ions of interest to x-ray laser plasmas. The calculations were carried out over a large range of incident electron energy starting from near the threshold of the particular electronic transition considered.

Individual contributions of the partial waves are listed in Table 1 to illustrate the variation of partial scattering cross-section with increasing angular momentum. Examination of Table 1 shows that for each set of energy, the partial cross-section first increases with increasing l, peaks at an intermediate l value and falls off gradually at higher l. The total cross-section has the highest value near threshold and decreases slowly with increasing electron energy. This feature is also seen from variation of collisional excitation cross-sections with incident electron energy for the other transitions of Li-like Al as shown in Tables 2 and 3.

Electron collisional excitation rate coefficients were also calculated for different transitions over a range of temperature appropriate for x-ray laser plasmas and typical z-pinch plasmas. The excitation rates were obtained by integrating the calculated cross-sections weighted by the Maxwell-Boltzmann distribution over the entire energy range. As seen from Tables 4, 5 and 6, the excitation rate coefficients initially increase rapidly with temperature, goes through a peak and decreases slowly with increasing temperature. The maximum of excitation rates indicates the temperature at which electron collisional excitation can substantially populate the upper levels leading to population inversion and lasing.

Calculations for other ions of lithium isoelectronic sequence such as CIV have also been done. We will briefly discuss the main aspects of those results. Burke et al[14] were

the first to apply the close-coupling method to lithium like ions. For CIV, calculation of 2s→2p collision strengths show satisfactory agreement between theory and experiment.

Exchange effects turn out to be important for CIV from comparison with experimental data. Distorted Wave without exchange calculations give results that are at least 15% higher than experimental data. 2-state close-coupling calculations, on the other hand, agree with the experimental data very well.

The effect of coupling to higher states for 2s→2p collision strength calculation is much less in CIV compared to, for example Li-like Be. Since the energy difference between 2s and 2p states increases linearly with Z and the energy difference between 2s and higher n states increases approximately as Z^2, the coupling becomes less important as Z increases. The average effect of resonance contribution to collision strength is an enhancement of 3% in the energy region below the n=3 levels. Resonances are found to have the most significant effect on D-wave (l=2) contribution which are small compared with the total collision strength.

IV. CONCLUSIONS

Accurate calculations of electron collisional excitation and ionization cross-sections and rate coefficients of different atoms and ions are important input to overall atomic modeling of radiative properties of plasmas. It is particularly useful in the context of collisional excitation scheme for x-ray lasers. In most investigations to achieve lasing with ionized plasmas of different z, available experimental data for collisional cross-sections and rates are limited. Thus, the necessary data have to be provided by theoretical calculations. The Distorted Wave with exchange method is seen to be a reliable and speedy technique for the purpose. In specific cases, such as near the threshold for low Z elements, close-coupling calculations can provide data of high accuracy. The present work on collisional processes, (along with our previous work on photoionization, photoexcitation, radiative decay and recombination processes) forms a useful component for the overall atomic modeling capability for x-ray laser and laboratory plasmas.

At very low plasma density, collisional excitation and deexcitation rates are small, radiative decay is then a dominant process. As the plasma density increases, the collisional rates increase rapidly and collisional radiative equilibrium can exist. These in turn, have their effects on the relative abundance of ionic populations as well as on the population inversion of levels and thus affect lasing. The modification of collisional excitation and ionization cross-sections etc. with increasing plasma density, therefore, is an additional problem area that requires further investigation. In the present 6-month project; this aspect has not been addressed. Preliminary calculations, using screened atomic potential to include the plasma effects, indicate, however, that for typical x-ray laser plasma condition (with electron density 10^{20} - 10^{21} cm^{-3} and for highly stripped, high Z ions), the collisional ionization cross-sections are modified by only a few percent. For low Z ions with a large

number of bound electrons (such as Neon-like ion with 10 electrons per ion) and at higher plasma density, the modifications to cross-sections and rates may be substantial.

V. REFERENCES

1. A.G. Molchanov, Usp. Fiz. Nauk 106, 165(1972) [Sov. Phys-Usp. 15, 124 (1972).

2. M.A. Duguay, Laser Focus, 9, 41(1973).

3. R.C. Elton, NRL Memo Report No. 2799(1974).

4. R.C. Elton, Appl. Opt. 14, 97(1975).

5. A.N. Zherikin, et. al. Sov. J. Quantum Electron, 6, **82**(1976).

6. K. G. Whitney et. al., J. Appl. Phys. 46, 4103 (1975).

7. D.L. Mathews et. al., Phys. Rev. Lett, 54, 110(1985).

8. M.D. Rosen et al., Phys. Rev. Lett. 54, 106(1985).

9. J. Davis JQSRT 14, 549(1974)

10. See, for example, M. Blaha et. al., JQSRT, 16, 1043(1976).

11. For a review, see, for example, B.L. Moiseiwitsch & S.J. Smith, Reviews of Modern Physics, 40, No. 2., p. 237 (1968).

12. J.C. Slater, Phys. Rev. 81, 385(1951).

13. U. Gupta, Project Report submitted to the AFOSR, "Modeling of Atomic Processes for X-ray Laser Plasmas", BRA-88-W010R (1987).

14. P.G. Burke et. al., J. Phys. B 2, 1142(1969).

15. U. Gupta and A.K. Rajagopal, Review Article in Physics Reports, 82, No. 6 (North Holland Publishing Co.)(1982)

TABLE 1

Li-like Aℓ XI

Electronic Transition: $1s^2 3d$, $^3D \rightarrow 1s^2 4s$, ^2S

Energy of Incident Electron (Ryd)	Energy of Outgoing Electron (Ryd)	Angular Momentum	Partial Scattering Cross-Section	Total Collision Strength	Scattering Cross-Section (πa_0^2)
78.17	1.36	0	0.2124E-03	0.7374 E-01	1.13 E-19
		1	0.3074E-02		
		2	0.8544E-02		
		3	0.1811E-01		
		4	0.2543E-01		
		5	0.7966E-02		
		6	0.6874E-02		
		7	0.2589E-02		
		8	0.6871E-03		
116.57	39.76	0	0.1335E-03	0.6738 E-01	6.92 E-20
		1	0.2254E-02		
		2	0.5444E-02		
		3	0.1232E-01		
		4	0.2346E-01		
		5	0.4668E-02		
		6	0.7656E-02		
		7	0.5692E-02		
		8	0.3073E-02		
		9	0.1431E-02		
154.98	78.17	0	0.8864E-04	0.6344 E-01	4.90 E-20
		1	0.1742E-02		
		2	0.3829E-02		
		3	0.8646E-02		
		4	0.2116E-01		
		5	0.3589E-02		
		6	0.5929E-02		
		7	0.6469E-02		
		8	0.4824E-02		
		9	0.3037E-02		
		10	0.1749E-02		

TABLE 1 (Cont'd)

Li-like Aℓ XI

Electronic Transition: $1s^2 3d$, $^3D \rightarrow 1s^2 4s$, ^2S

Energy of Incident Electron (Ryd)	Energy of Outgoing Electron (Ryd)	Angular Momentum	Partial Scattering Cross-Section	Total Collision Strength	Scattering Cross-Section (πa_0^2)
		0	0.4249E-04		
		1	0.1156E-02		
		2	0.2303E-02		
		3	0.4646E-02		
231.79	154.98	4	0.1618E-01	0.6011	3.10
		5	0.4792E-02	E-01	E-20
		6	0.3121E-02		
		7	0.4878E-02		
		8	0.5310E-02		
		9	0.4692E-02		
		10	0.3645E-02		
		11	0.2622E-02		
		0	0.2228E-04		
		1	0.8410E-03		
		2	0.1612E-02		
		3	0.2815E-02		
		4	0.1179E-01	0.5740	2.23
308.60	231.79	5	0.6131E-02	E-01	E-20
		6	0.2678E-02		
		7	0.3271E-02		
		8	0.4132E-02		
		9	0.4474E-02		
		10	0.4225E-02		
		11	0.3595E-02		
		12	0.2857E-02		
		13	0.2166E-02		
		0	0.1231E-04		
		1	0.6489E-03		
385.41	308.60	2	0.1231E-02	0.5635	1.75
		3	0.1912E-02	E-01	E-20
		4	0.8508E-02		
		5	0.6468E-02		
		6	0.3196E-02		
		7	0.2688E-02		
		8	0.3081E-02		
385.41	308.60	9	0.3607E-02	0.5635	1.75
		10	0.3896E-02	E-01	E-20
		11	0.3787E-02		
		12	0.3373E-02		
		13	0.2787E-02		
		14	0.2269E-02		
		15	0.1808E-02		

TABLE 1 (Cont'd)

Li-like Aℓ XI

Electronic Transition: $1s^2 3d$, $^3D \rightarrow 1s^2 4s$, ^2S

Energy of Incident Electron (Ryd)	Energy of Outgoing Electron (Ryd)	Angular Momentum	Partial Scattering Cross-Section	Total Collision Strength	Scattering Cross-Section (πa_0^2)
		0	0.3989E-05		
		1	0.4329E-03		
		2	0.8266E-03		
		3	0.1151E-02		
		4	0.4578E-02		
		5	0.5434E-02	0.6162	1.37
539.04	462.22	6	0.4044E-02	E-01	E-20
		7	0.3049E-02		
		8	0.2501E-02		
		9	0.2368E-02		
		10	0.2622E-02		
		11	0.2981E-02		
		12	0.3179E-02		
		13	0.3046E-02		
		14	0.2837E-02		
		15	0.2520E-02		
		0	0.8388E-06		
		1	0.2789E-03		
		2	0.5441E-03		
		3	0.7673E-03		
		4	0.2118E-02		
		5	0.3348E-02		
769.47	692.66	6	0.3663E-02	0.3276	5.10
		7	0.3565E-02	E-01	E-21
		8	0.3109E-02		
		9	0.2435E-02		
		10	0.1930E-02		
		11	0.1818E-02		
		12	0.2016E-02		
		13	0.2213E-02		
		14	0.2437E-02		
		15	0.2515E-02		

TABLE 2

Li-like Aℓ XI

Electronic Transition: $1s^2 2s,\ ^2S \rightarrow 1s^2 3S,\ ^2S$

Energy of Incident Electron (Ryd)	Energy of Outgoing Electron (Ryd)	Total Collision Strength	Scattering Cross-Section (πa_0^2)
252.58	1.36	0.9397E-01	2.23E-19
378.19	126.97	0.9070E-01	1.44E-19
503.80	252.58	0.8874E-01	1.05E-19
755.02	503.80	0.8633E-01	6.84E-20
1006.25	755.02	0.8484E-01	5.05E-20
1257.47	1006.25	0.8380E-01	3.99E-20
1759.91	1508.69	0.8243E-01	2.80E-20
2513.57	2262.35	0.8123E-01	1.93E-20

TABLE 3

Li-like Aℓ XI

Electronic Transition: $1s^2 3s,\ ^2S \rightarrow 1s^2 3d,\ ^2D$

Energy of Incident Electron (Ryd)	Energy of Outgoing Electron (Ryd)	Total Collision Strength	Scattering Cross-Section (πa_0^2)
86.53	1.36	0.4201E+00	2.91E-18
129.12	43.95	0.4223E+00	1.96E-18
171.71	86.53	0.4232E+00	1.47E-18
256.88	171.71	0.4228E+00	9.85E-19
342.06	256.88	0.4221E+00	7.38E-19
427.23	342.06	0.4211E+00	5.90E-19
597.58	512.40	0.4191E+00	4.20E-19
853.10	767.93	0.4165E+00	2.92E-19

TABLE 4

Li-like Aℓ XI

Electronic Transition: $1s^2 3s, {}^2S \rightarrow 1s^2 3d, {}^2D$

Temperature (OK)	Excitation Rate Coefficient $cm^3 sec^{-1}$
3.50E+05	1.39E-12
5.80E+05	1.82E-10
8.10E+05	4.35E-10
1.00E+06	5.97E-10
1.20E+06	6.78E-10
3.50E+06	7.30E-10
5.80E+06	7.32E-10
8.10E+06	6.35E-10
1.00E+07	5.63E-10
3.50E+07	4.80E-10

TABLE 5

Li-like Aℓ XI

Electronic Transition: $1s^2 2s, {}^2S \rightarrow 1s^2 3s, {}^2S$

Temperature (OK)	Excitation Rate Coefficient $cm^3 sec^{-1}$
3.50E+05	3.28E-20
5.80E+05	1.64E-13
8.10E+05	3.44E-12
1.00E+06	1.21E-11
1.20E+06	2.15E-11
3.50E+06	3.18E-11
5.80E+06	8.94E-11
8.10E+06	9.51E-11
1.00E+07	9.18E-11
3.50E+07	8.37E-11

TABLE 6

Li-like Aℓ XI

Electronic Transition: $1s^2 3d, {}^2D \rightarrow 1s^2 4s, {}^2S$

Temperature (OK)	Excitation Rate Coefficient $cm^3 sec^{-1}$
3.50E+05	1.07E-13
5.80E+05	7.93E-12
8.10E+05	1.65E-11
1.00E+06	2.11E-11
1.20E+06	2.31E-11
3.50E+06	2.42E-11
5.80E+06	2.06E-11
8.10E+06	1.62E-11
1.00E+07	1.33E-11
3.50E+07	1.04E-11